Line parameters including temperature dependences of self- and air-broadened line shapes of $^{12}C^{16}O_2$: 1.6-μm region

V. Malathy Devi[a,*], D. Chris Benner[a], Keeyoon Sung[b], Linda R. Brown[b], Timothy J. Crawford[b], Charles E. Miller[b], Brian J. Drouin[b], Vivienne H. Payne[b], Shanshan Yu[b], Mary Ann H. Smith[c], Arlan W. Mantz[d], Robert R. Gamache[e]

[a]*Department of Physics, The College of William and Mary, Box 8795, Williamsburg, VA 23187, USA*
[b]*Jet Propulsion Laboratory, California Institute of Technology, 4800 Oak Grove Drive, Pasadena, CA 91109, USA*
[c]*Science Directorate, NASA Langley Research Center, Hampton, VA 23681, USA*
[d]*Department of Physics, Astronomy and Geophysics, Connecticut College, New London, CT 06320, USA*
[e]*Office of the Academic Affairs, Student Affairs, International Relations, University of Massachusetts, One Beacon Street, Boston, MA 02108, USA*

Number of pages: **46**
Number of Figures: **15**
Number of Tables: **8**
Supplemental files: 1

[a] Corresponding author
Dr. V. Malathy Devi
Phone: 757.864.5521
Fax: 757-864-4343
e mail: malathy.d.venkataraman@nasa.gov

Abstract

Pressure-broadened line shapes in the 30013←00001 ($\nu_1+4\nu_2^0+\nu_3$) band of $^{12}C^{16}O_2$ at 6228 cm^{-1} are reanalyzed using new spectra recorded with sample temperatures down to 170 K. High resolution, high signal-to-noise (S/N) laboratory measurements of line shapes (Lorentz air- and self-broadened half-width coefficients, pressure-shift coefficients and off-diagonal relaxation matrix element coefficients) as a function of gas sample temperatures for various pressures and volume mixing ratios are presented. The spectra were recorded using two different Fourier transform spectrometers (FTS): (1) the McMath-Pierce FTS located at the National Solar Observatory on Kitt Peak, Arizona (and reported in Devi et al., J Mol Spectrosc 2007;245:52-80) and, (2) the Bruker IFS-125HR FTS at the Jet Propulsion Laboratory in Pasadena, California. The 19 spectra taken at Kitt Peak were all recorded near room temperature while the 27 Bruker spectra were acquired both at room temperature and colder temperatures (170-296 K). Various spectral resolutions (0.004-0.011 cm^{-1}), absorption path lengths (2.46 m-121 m) and CO_2 samples (natural and ^{12}C-enhanced) were included in the dataset. To maximize the accuracies of the various retrieved line parameters, a multispectrum nonlinear least squares spectrum fitting software program was used to adjust the ro-vibrational constants (*G*,*B*,*D* etc.) and intensity parameters (including Herman-Wallis terms) instead of directly measuring the individual line positions and intensities. To minimize systematic residuals, line mixing (via off-diagonal relaxation matrix elements) and quadratic speed dependence parameters were included in the analysis. Contributions from other weakly absorbing bands: the 30013←00001 and 30012←00001 bands of $^{13}C^{16}O_2$, the 30013←00001 band of $^{12}C^{16}O^{18}O$, hot bands 31113←01101 and 32212←02201 of $^{12}C^{16}O_2$, as well as the 40013←10001 and the 40014←10002 bands of $^{12}C^{16}O_2$, present within the fitted interval were also measured. Results from previous works and new calculations are compared to present measurements, where appropriate.

Key words: CO_2, Lorentz width, pressure shift, temperature dependence, relaxation matrix element coefficients, speed dependence

1. Introduction

The present study was undertaken to support space-based observations of carbon dioxide. Both the Orbiting Carbon Observatory-2 (OCO-2) [**1-3**], launched in 2014, and the Japanese Greenhouse Gases Observing Satellite (GOSAT) [**4**], launched in 2009, rely on measurements of the absorption of reflected sunlight in the 1.61 μm and 2.06 μm CO_2 bands and the 0.76 μm O_2 A band. From these measurements, estimates of the column-averaged dry air mole fraction, X_{CO2}, can be retrieved [*e.g.*, **5**,**6**]. The X_{CO2} fields can then be used within atmospheric inversion frameworks to infer sources and sinks of CO_2. Systematic errors in the retrievals can introduce regional or airmass-dependent biases in the atmospheric inversions that affect the estimates of the sources and sinks [**7**]. The goal for the OCO-2 mission is to provide atmospheric X_{CO2} fields with 0.25 % precision [**4**] (1 part in 400). This goal places stringent demands on the molecular absorption model used within the retrievals. The accuracy of the molecular absorption model is determined by the accuracy of the line parameters and line shape used, and the critical need for accurate spectroscopic parameters for the near infrared (NIR) CO_2 bands has been clearly demonstrated in previous work [**8**].

This study focuses on accurate measurements of spectroscopic line parameters at 1.6 μm. The strongest band in this region is the 30013←00001 band of $^{12}C^{16}O_2$ at 6228 cm^{-1}, followed by its first hot band (31113←01101)(*e*,*f*) at 6196 cm^{-1}. Weaker absorption lines of $^{13}C^{16}O_2$ (30013←00001 and 30012←00001) and $^{12}C^{16}O^{18}O$, (30013←00001) also appear between 6120 and 6280 cm^{-1}. The remaining three $^{12}C^{16}O_2$ bands are weaker: a second hot band 32213←02201(*e*,*f*), 40014←10002 and 40013←10001. Transitions from minor isotopologues (such as $^{12}C^{16}O^{18}O$, $^{13}C^{16}O^{18}O$) also contribute detectable absorption in this wavelength region.

Due to the importance in remote sensing applications, there have been a very large number of measurements reported for CO_2 in the 1.6 μm region [**9**-**32**]. The spectral region between 4600 cm^{-1} and 7000 cm^{-1} was previously studied by Toth et al. [**13-17**] by analyzing a large number of high-resolution, high signal to noise (S/N) spectra recorded using the McMath-Pierce Fourier transform spectrometer (FTS) at Kitt Peak. Those spectra were obtained using samples of CO_2 in natural isotopologue abundance, high-purity ^{12}C-enriched CO_2, ^{13}C-enriched CO_2 and ^{18}O-enriched CO_2. The analyses of those data were carried out using a Voigt line shape and a spectrum-by-spectrum fitting procedure. Later, we reinvestigated two of the Fermi tetrad band regions (located at 6228 cm^{-1} and 6348 cm^{-1} respectively) [**18,19**]. Our published results for the 30013←00001 and 30012←00001 band regions [**18,19**] applied the multispectrum fitting technique [**33,34**] with non-Voigt line shapes: line

mixing using the off-diagonal relaxation matrix elements [**35**] and quadratic speed dependence [**36**]. In **Table 1** we give an overview of line shape measurements reported since 2006 for the 30013←00001 band, including the studies published after our previous measurements [**18**] and results by Toth et al. [**14**] for self-broadened half-width and pressure-shift coefficients. However, all our prior efforts involved gas samples at room temperature, and further laboratory study of pressure broadening as a function of temperature was required for accurate atmospheric remote sensing by OCO-2.

In the present study (**PS**), we expand our earlier study [**18**] to include similar high-quality spectra of pure and air-broadened CO_2 samples recorded at different gas sample temperatures (170−296 K) and pressures. The range of measurement conditions was designed to span the range of temperatures and pressures encountered in Earth's atmosphere.

Table 1 prior studies comes here (landscape format)

2. Experimental Details

A total of 46 spectra were analyzed in this work. Nineteen were recorded [**18**] at room temperature using the McMath-Pierce FTS at the National Solar Observatory on Kitt Peak, AZ. The 27 additional laboratory spectra were recorded using the Bruker 1FS-125 HR FTS at JPL using a temperature-controlled gas sample cell at various temperatures between ~170 and 250 K. For these measurements, each FTS (McMath-Pierce and JPL) was configured with a CaF_2 beamsplitter and InSb detectors. A quartz halogen lamp was the light source for the McMath-Piece FTS while a tungsten lamp was used for the Bruker IFS-125HR at JPL. The source aperture and filter band pass varied between the two arrangements. The instrumental setups and configuration details are given in **Table 2**, and the experimental conditions for the individual spectra are provided in **Table 3**.

Table 2 (FTS setups) appears here

For the Kitt Peak spectra, the absorption path lengths ranged between 2.46 and 121 m for 13 pure CO_2 spectra and six air-broadened CO_2 spectra. All spectra were recorded with a natural CO_2 sample except

for three obtained with a 99.99% ^{12}C-enriched CO_2 sample. The 27 cold spectra from the JPL Bruker FTS include 11 pure CO_2 spectra and 16 spectra of CO_2 broadened by dry air (*Ultra Zero* grade from Airgas). All of the JPL spectra were taken with the multipass Herriott cell [**37**] which has a fixed path length of 20.941(6) m. The high-purity (99.99% ^{12}C-enriched) CO_2 sample was used for all of the JPL spectra to simplify the retrievals by minimizing interferences due to absorption features arising from the rarer isotopologues (*e.g.* $^{13}C^{16}O^{16}O$, $^{12}C^{16}O^{18}O$). In the Kitt Peak spectra, weak features of $^{13}C^{16}O_2$ and $^{12}C^{16}O^{18}O$ isotopologues were observed mostly in longer absorption path length (~25 and 49 m) spectra using the high-purity natural sample of CO_2. For these two species, the isotopologue abundances were determined individually and applied in each fitted spectrum. For all other rarer isotopologues, their natural abundances listed in the HITRAN database [**38-40**] were used.

For the 24 self-broadened spectra (13 from Kitt Peak and 11 from JPL), the sample pressures ranged between 11 Torr and 897 Torr; for the 22 air-broadened CO_2 spectra the total sample pressures varied from 50 Torr to 924 Torr with the CO_2 volume mixing ratios in the 0.03-0.40 range. It should be noted that the lowest pressure pure sample spectrum with 11.04 Torr was included in the analysis to provide "zero-pressure" line positions. The CO_2 spectra listed in **Table 3** were taken over a wide temperature range from 170 to 297 K, for which more than half the scans (11 pure sample and 16 air-broadened) were obtained at temperatures below 293 K.

Additional care was taken to achieve consistency in the low-temperature data. For instance, at least 20 minutes were allowed for each new gas fill to reach temperature and pressure stabilization prior to starting their scanning. Sample pressures and temperatures were monitored continually during the entire scanning period using PRT temperature sensors and MKS Baratron transducers for pressure readings. The pressure gauges were calibrated regularly and the recommended calibration factors provided by the manufacturers were used for the temperature sensors. The interferograms were collected approximately every 10 minutes and then transformed individually before being included in the final averaged spectrum. Other details about characterization of instrumental line shape function for the Bruker FTS at JPL, the coolable Herriott cell system, and experimental precautions taken to minimize systematic errors have been provided in Refs. [**9,37**] and references therein.

Table 3 comes next (gas conditions by run)

Calibrations for line positions from Kitt Peak CO_2 spectra were performed with respect to two sets of secondary standards (the 2←0 band of CO [**41**] or the $\nu_1+\nu_3$ band of C_2H_2 [**42**]) whose spectra were obtained by inserting a second absorption cell in the beam's path [**17-19**]. For the Bruker spectra taken at JPL, a 10-cm cell containing low pressure of HCl was inserted in the optical path just before the detector, and the 2←0 line positions of HCl from HITRAN2008 [**39**] were used as the reference standard. The relative calibration factors of all the Bruker spectra were tied to that of a single Bruker spectrum (since HCl lines appear the same in all spectra they are independent of sample gas in absorption cell containing CO_2); any differences between the calibration scales of spectra from the Kitt Peak McMath-Pierce FTS and the JPL Bruker FTS were removed by adjusting the calibration correction factor of that single Bruker spectrum to which all other Bruker FTS data were constrained, in order to obtain an internally consistent set of line positions from spectra recorded by the two different instruments. We estimate the overall absolute uncertainty in our retrieved line positions to be better than ±0.0001 cm^{-1}. Further details on line position comparisons are given in **Section 4.1**.

3. Spectral retrievals and measurements

The multispectrum fit in the present study was initiated using results from our previous study [**18**]. To reduce the redundancy in gas conditions we selected 19 spectra from the original set of 26 room-temperature spectra in Ref. [**18**] and added the 27 new Bruker low-temperature spectra one at a time until all 46 spectra were included in the multispectrum fit.

3.1. Line positions and intensities

Line positions and intensities of the stronger individual bands were obtained by adjusting the ro-vibrational constants and band intensity parameters using well-known theoretical quantum mechanical expressions as part of the nonlinear least squares minimization. For individual line positions, ν_i, and intensities, S_i, three equations (**1-3**) were used to solve for the ro-vibrational **(1)** G, B, D, H and transition moment constants **(2)** vibrational band strength S_v, and **(3)** the Herman-Wallis type parameters a_1, a_2, a_3 and a_4).

$$\nu_i = G' - G'' + (B'J'[J'+1] - D'\{J'[J'+1]\}^2 + H'\{J'[J'+1]\}^3)$$
$$-(B''J''[J''+1] - D''\{J''[J''+1]\}^2 + H''\{J''[J''+1]\}^3) \quad (1)$$

$$S_i = \frac{S_v \nu_i L_i F}{Q_r \nu_0} \; exp\left(\frac{-C_2 E''}{T_0}\right)\left[1 - exp\left(\frac{-C_2 \nu_i}{T_0}\right)\right] \quad (2)$$

where,

$$F = (1 + a_1 m + a_2 m^2 + a_3 m^3 + a_4 J(J+1)^2 \quad (3)$$

and, m = -J'' for P-branch and J''+1 for R-branch lines. ν_0 is the band center (equal to G'-G''), ν_i and S_i correspond, respectively, to the transition wavenumber (cm^{-1}) and the intensity in cm/(molecule of the i^{th} line, where prime and double prime refer to the upper and lower levels; J is the rotational quantum number. The lower state ro-vibrational constants were constrained to be the values given by Miller and Brown [**29**] for $^{12}C^{16}O_2$ and $^{16}O^{12}C^{18}O$ and by Miller et al. [**30**] for $^{13}C^{16}O_2$. In **Eq. (2)**, E'' is the lower state energy and T_0 is the reference temperature (296 K). L_i are the Hönl-London factors, S_v is the vibrational band strength and, C_2 is the second radiation constant. The values of the rotational quantum partition function, Q_r, at T=296 K are 263.87063 for $^{12}C^{16}O_2$, 527.71608 for $^{13}C^{16}O_2$ and 559.30454 for $^{12}C^{16}O^{18}O$ [**43**]. We note that in our previous studies [**18,19**] a slightly different Q_r value (263.60) was used for $^{12}C^{16}O_2$, contributing to a change in the vibrational band strength S_v by 0.10% (**Table 6**) in the present study. The slight change in the vibrational band strength (S_v) value (0.16%) between PS and [18] is attributed due to small changes in the various retrieved spectral line parameters and the different sets of spectra used in the two analyses.

In practice, the multispectrum fitting computes the line positions and line intensities of the bands for which individual constraints are activated. The positions and intensities are calculated up to the highest rotational quantum numbers for which the constraints are applied. This technique is particularly important when absorption features are weak (*e.g.*, high-J transitions), blended or overlapped with other neighboring features. Recall that these "calculated" line positions and intensities are actually determined from the ro-vibrational and intensity parameters obtained from present "measured" values applying the multispectrum fitting. These calculated values are useful to extrapolate the measurements to a few higher J transitions beyond the experimentally measured lines using the constraints. The extrapolated position and intensity values beyond a reasonable J outside of the measured transitions

should be used with caution, especially when the band in question is perturbed by known or unknown local or non-local resonances. As will be shown later, for the Herman-Wallis factors, we found that the a_1, a_2 and a_3 terms were sufficient to describe the strongest 30013←00001 band while only a_1 and a_2 were needed for three hot bands (31113←01101, 40014←10002 and 40013←10001). For the weakest hot band 32213←02201, only the a_1 term could be determined. In practice, the a_4 term can be separated from the a_2 term only when a Q branch is present and measurable, and was retained in Eq. (**3**) for the sake of completeness.

3.2. Pressure-broadened line shapes

Similar to our previous analyses (*e.g.*, [**18,19**]), the air- and self-broadened Lorentz half-width and pressure-shift coefficients and their temperature dependences defined in **(4)**-**(6)**, were measured on a line-by-line basis using the constrained multispectrum least squares fittings [**33**].

$$b_L(p,T) = p\left[b_L^0(air)(p_0,T_0)(1-\chi)\left[\frac{T_0}{T}\right]^{n1} + b_L^0(self)(p_0,T_0)\chi\left[\frac{T_0}{T}\right]^{n2}\right] \quad (4)$$

$$\nu = \nu_0 + p\left[\delta^0(air)(1-\chi) + \delta^0(self)\chi\right] \quad (5)$$

$$\delta^0(T) = \delta^0(T_0) + \delta'(T - T_0) \quad (6)$$

In Eqs. **(4) – (6)**, b_L^0 and δ^0 represent pressure broadening and pressure-shift coefficients (in cm^{-1} atm^{-1} at 296 K), respectively. $b_L(p, T)$ is the Lorentz half-width (in cm^{-1}) of the spectral line at pressure p and temperature T, and b_L^0 $(Gas)(p_0, T_0)$ is the Lorentz half-width coefficient of the line at the reference pressure p_0 (1 atm) and temperature T_0 (296 K) of the broadening gas (either air or CO_2), and χ is the ratio of the partial pressure of CO_2 to the total sample pressure in the cell. Temperature dependences of air- and self-broadened half-width coefficients, b_L^0 (air) (p_0, T_0) and b_L^0 $(self)$ (p_0, T_0), and pressure-induced shift coefficients, δ'(air) and δ'(self) were determined separately for each transition from the same fit. As shown in **Eq. (6)** a linear model was used for the temperature dependence of pressure shift coefficients.

The final multispectrum fit of all 46 spectra at different optical densities and temperatures is shown in **Fig. 1**. The bottom panel **Fig. 1(f)** displays all 46 individual observed spectra that were fitted simultaneously. Since the emphasis for our new study is to determine temperature dependences of

pressure-broadening, the residuals shown in the top five panels **(a)**-**(e)** are grouped by the different temperature ranges; these are the corresponding weighted fit residuals (observed minus calculated) for the air- and self-broadened spectra recorded with the two spectrometers. As in previous studies, a maximum weight of 1.0 was assigned to the spectrum with the highest S/N, while for each other spectrum the weight was set inversely proportional to the square of the ratio of the S/N of that spectrum to the S/N of the spectrum with the highest weight. No significant differences in the residuals from the various spectra are seen, thus confirming that proper weighting scheme has been applied. A shorter spectral interval (6220-6235 cm^{-1}) covering the range of P8-R8 lines taken from **Fig. 1** is re-plotted in **Fig. 2** to show the details around the center of the strongest 30013←00001 band.

Insert Figs. 1 and 2 here

The multispectrum fits of all 46 spectra shown in **Figs. 1** and **2** correspond to the retrieval for the entire P and R branches of 30013←00001 band as well as other weaker bands in the 6120-6280 cm^{-1}. During the fittings, the Lorentz half-width and pressure-shift coefficients and their temperature dependences were slowly released, for a few lines at a time, then high pressure and low temperature spectra were added to the least squares solution. We note that in our analysis, the internal consistencies of the CO_2 volume mixing ratios for each of the air-broadened spectra were closely inspected, and were carefully adjusted to minimize the fit residuals. The quantitative adjustments made to the volume mixing ratios of CO_2 in air-broadened spectra should not be a huge concern because (1) line intensities were measured by simultaneously fitting a number of key pure CO_2 spectra with known isotopologue abundances without changing pressures and temperatures which determined the calibration of the line intensities and, (2) we did not use premixed samples of CO_2 and air; CO_2-air mixtures were prepared by adding air to pre-measured amounts of CO_2 already installed in the cell. Details about absolute uncertainties are discussed later in a separate section. Adding weak absorption features from the other seven bands appearing in this region alone did not remove the fit residuals completely until speed dependence and line mixing via relaxation matrix elements were also considered in the fit. The solid horizontal line at the bottom of **Figs. 1(f)** and **2(f)** corresponds to 100% absorption. The short vertical lines at the top of **Figs. 1(f)** and **2(f)** indicate positions of absorption lines included in the fit.

Table 4 (the count of types of retrieved parameters) comes here

The total numbers of measured parameters retrieved in this work are summarized in **Table 4**. For the positions and intensities, these include 74 transitions (P74-R72) for the 30013←00001 band of $^{12}C^{16}O_2$, 136 transitions (P59*e*-P3*e*, Q17*e*-Q1*e*, R3*e* -R59*e*; P60*f*-P2*f*, Q16*f*-Q2*f*, R2*f*-R60*f*) of the 31113←01101 (*e* and *f* components) band of $^{12}C^{16}O_2$, 41 lines (P40*e*-R39*f*) for the 32213←02201 (*e* and *f* components) band of $^{12}C^{16}O_2$, 50 transitions (P48-R50) for the 40014←10002 band of $^{12}C^{16}O_2$, 47 lines (P46*e*-R46*e*) of the 40013←10001 band of $^{12}C^{16}O_2$, 48 lines (P46-R48) for the 30013←00001 band of $^{13}C^{16}O_2$, 56 transitions (P54-R54) for the 30012←00001 band of $^{13}C^{16}O_2$, and 45 transitions (P10-R41) for the 30013←00001 band of $^{12}C^{16}O^{18}O_2$. The remaining weak lines (fragmentary bands or without assignments) were added during the fitting process; those positions and intensities were also measured but not included in the **Supplemental list**. It may be recalled that, except for several spectra recorded at Kitt Peak using a natural CO_2 sample, all the remaining spectra in **Table 3** were obtained using either a 99.99% ^{12}C-enriched CO_2 or CO_2 samples mixed with air. Thus, the line intensities listed for $^{13}C^{16}O_2$ and $^{12}C^{16}O^{18}O$ in the **Supplemental file** are thought to be a few percent less accurate, but nevertheless could be determined with sufficient precision to obtain the best overall multispectrum fit. For the natural CO_2 sample, abundances for the various isotopologues listed in the HITRAN [**38-40**] database were used. For the ^{12}C-enriched samples, the isotopologue abundances (minor species) were determined for each spectrum from least squares fittings to match the intensities in all spectra fit simultaneously. In the sections that follow, we compare our new measurements with our prior room-temperature results and HITRAN. All individual measurements are given in the **Supplemental file** for four bands of $^{12}C^{16}O_2$, two bands of $^{13}C^{16}O_2$ and one band of $^{12}C^{16}O^{18}O$. We note that many entries contain only the positions and room temperature intensities of weaker lines, and those for the 30013←00001 band of $^{13}C^{16}O_2$ and the 40013←10002 band of $^{12}C^{16}O_2$ are often extrapolated values calculated by our multispectrum fitting; these are included to indicate all of the lines incorporated in the fits in order to retrieve the target line shape parameters of main bands in this spectral region.

Table 5 sample (selected measures) comes here (landscape)

A portion of the measured line parameters (P40 through R40) for the 30013←00001 band of $^{12}C^{16}O_2$ are given in **Table 5**. The table lists the line identification in the first column followed by the calculated line position (cm^{-1}) and the calculated line intensity (cm/molecule) at 296 K (determined from the retrieved ro-vibrational and intensity parameters by the least squares fits). The two-row format for line shape parameters of each transition indicates air-broadening parameters in the upper row and self-broadening values in the lower row; these are the measured broadening coefficient (cm^{-1}/atm^{-1}) at 296 K for both air- and self-broadening, b_L^0 (air) and b_L^0 (self), the temperature dependence exponents (n_1 and n_2) for air- and self-broadening, respectively (no units), air- and self- pressure-shift coefficient (cm^{-1} atm^{-1} at 296 K), δ^0(air) and δ^0(self), and their temperature dependence coefficients (in cm^{-1} atm^{-1} K^{-1}), δ'(air) and δ'(self), respectively. We note that only one speed dependence parameter (per transition) common to both broadening gases is reported, and it is assumed to be independent of the sample temperatures. The uncertainties in line positions, pressure-shift coefficients and their temperature dependences are listed in parentheses (in units of the last quoted digit) next to their values; % uncertainties are provided for line intensities, Lorentz half-width coefficients, the Lorentz half-width temperature dependence exponents and the speed dependence parameters; these are listed in the columns next to their values. The uncertainties listed in **Table 5** and in the **Supplemental file** correspond to the one-sigma internal statistical uncertainties from the multispectrum fittings. However, these values are not considered to represent the absolute uncertainties because there may be systematic uncertainties arising from additional sources, such as the uncertainties in the experimental physical conditions of spectra, wavenumber calibration errors, and other spectrum parameters such as zero level, residual phase errors and field of view corrections.

4. Discussion of results and comparison with databases

The CO_2 line parameters at 1.6 μm were revised in the last three editions of the HITRAN database [**38-40**]. For HITRAN2004 [**38**], existing entries from the Direct Numerical Diagonalization (DND) technique [**44**] were replaced by combining selected experimental results with calculated line positions and intensities from the 2003 version of the Carbon Dioxide Spectroscopic Databank, CDSD-1000 [**45**]. Subsequently, the Toth et al. compilation [**17**] further improved the positions and intensities for HITRAN2008 [**39**]. In HITRAN2012 [**40**], the database has been greatly expanded using an updated CDSD-296 databank [**46**] to include line parameters for 12 CO_2 isotopologues, providing information not only for positions and intensities but also for air- and self-broadened Lorentz half-width

coefficients, temperature dependences of air-broadened half-width coefficients and air- pressure-induced shift coefficients. The CDSD-296 [**46**] line list includes CO_2 transitions with intensities as low as ~1 x10^{-30} cm^{-1}/(molecule cm^{-2}) at 296 K. Comparisons of present line parameters with the CDSD-296 [**46**] are shown in several graphs and are discussed in the section describing estimated total error budget. In addition to the CDSD-296 [**46**] databank, there are three other sources of spectroscopic information where line parameters are theoretically computed [**47–49**] with which present results are compared. In the following subsections we detail how our new $^{12}CO_2$ measurements for the 30013←00001 band compare with HITRAN values, selected laboratory measurements [*e.g.,* **Refs. 13,27,50**] and recent theoretical calculations [**46**–**49**].

4.1. Line positions

In **Fig. 3**, the mean differences in line positions from present work are compared to corresponding values from Toth et al. [**13**], seven R branch transitions reported by Long et al. [**27**] and three editions of the HITRAN database [**38**-**40**]; the position differenes are given in cm^{-1} vs. *m*. The Present Study (**PS**) and HITRAN values [**38**-**40**] extend from P74-R72, those from Toth et al. [**13**] cover the P60–R60 range, and from Long at al. [**27**] include 7 lines between R6 and R32. We recall that HITRAN2004 line parameters [**38**] were used as input to initiate our 2007 studies [**18**,**19**] and that the Toth et al. [**13**] values were included in the HITRAN2008 [**39**] update. We have also compared our present line positions with Majcherova et al. [**51**] who reported extensive measurements of the absorption spectrum of carbon dioxide in natural isotopologue abundance from spectra recorded with CW-cavity ring-down spectroscopy technique using several fibered DFB lasers in the 6132-6747 cm^{-1} interval. Spectroscopic parameters obtained from that study combined with selected experimental results from other measurements were used in updating the line positions for more than 29000 transitions for 364 bands using the effective Hamiltonian approach [**45**].

The systematic differences seen in **PS**-HITRAN2012 for transitions with $m > 60$ arise from extrapolating available predictions beyond the measured range; the discontinuities at $m = 62$, 64 and 74 are likely due to differences in combining files from different sources for HITRAN (see Ref. [**40**] for details). Specifically, in HITRAN2012, line positions from Toth et al. [**13**] were used for P46-R48 and for P48-P80 and R50-R84, the positions were obtained from experimental energy levels. These

experimental energy levels were in turn retrieved from measured line positions from several published studies using the RITZ computer code and applying Rayleigh-Ritz principle without any further modeling (for details see Ref. [**46**]). It may be that these procedures could be causing the *J* dependence in HITRAN not following a smooth pattern. The mean position differences between the **PS** and the values from all other studies compared are shown in **Fig. 3** and listed in the figure legend indicate very good agreement between the **PS** and all other studies. **Fig. 3** indicates the best agreement with a mean position difference of 0.00006 (1) cm^{-1} between **PS** and Long et al. [**27**] whose measurements were referenced to a cesium atomic clock via an optical frequency comb. If the comparisons were limited only to P60-R60 with all other studies, the mean position differences between **PS** and other studies would be close to the difference PS-Toth et al., since HITRAN2008 and HITRAN2012 used Toth et al. [**13**] measurements as discussed above. Recall that line positions reported in this study are "calculated" from the ro-vibrational parameters that were determined from the present "measured line positions" in applying the multispectrum fits. Including the position constraints allowed us to determine (calculate) positions of lines that are otherwise overlapped or blended and could not have been determinable.

Insert Fig. 3 here

In **Fig. 4** we have plotted two self-broadened spectra recorded with the longest optical path (49 m) and high pure CO_2 pressures of 896.84 and 252.42 Torr at ~294 K (see **Table 3**). In the top panel (a) the spectral interval from 6150–6270 cm^{-1} is plotted to show the overall strengths of all lines including the weak high *J* lines for the 30013←00001 band. In the middle panel (b) the spectral interval 6150–6170 cm^{-1} to include the weak high P(*J*) transitions while in the bottom panel (c) several weak high–R(*J*) transitions in the 6250-6270 cm^{-1} are shown; including assignments for some of these high–*J* lines. Higher *J* lines of the 30013←0001 band (beyond that are marked in **Fig. 4**) are not easily recognizable in this figure due to their weakness and blends with transitions from other neighboring bands. This figure illustrates some of the weakest transitions that were measured in the present study. These high *J* transitions are observable only at the high optical density spectra. By constraining the line positions and intensities using Eqs. (1)-(3), it was possible to measure those parameters for such weak and blended transitions that cannot otherwise be measured to the precisions achieved in this study. The plot indicates that by using longer absorption path, preferably CRDS spectra, it could be possible to

measure the positions and intensities of these weak and even weaker (higher J) transitions with better precision and accuracy. **Fig. 4** also confirms that the positions and intensities for transitions obtained by extrapolating the ro-vibrational and intensity parameters (**Table 6**) beyond the measured values of J could be less precise and therefore should be used with caution. In any experimental studies, the accuracies in calculated (or observed) positions and intensities are largely depended upon the highest J measured and hence on the H and L values determined for the ro-vibrational constants and, the F–factor parameters obtained from intensity measurements. These accuracies could in turn contribute to the level of deviations from zero difference for positions and unity for intensity ratios with other measurements/calculations.

Insert Fig. 4 (showing the weakest lines)

4.2. Intensities

Since the retrieved intensities for the various bands from the present study are nearly the same as those in our earlier room-temperature study [**18**], only the 30013←00001 $^{12}C^{16}O_2$ intensities are discussed in **Fig. 5**. The measured line intensities vs. m are plotted on both linear (**Fig. 5a)** and logarithmic (**Fig. 5b)** scales; since the error bars corresponding to the uncertainties are smaller than the size of the plot symbols in **Fig. 5(a)**, the uncertainties are plotted separately in **Fig. 5(b)**. For comparison, the HITRAN2012 [**40**] intensity values are also plotted as a solid curve in panels **(a)** and **(b)**. **Fig. 5(c)** shows the ratios (including error bars when appropriate) between the present values and those of Refs. [**13**,**39**,**40**], and the mean values of those ratios are given in the legend. The very small intensity uncertainties achieved in the present study are J-dependent because their values have been constrained using the theoretical quantum mechanical expressions and the uncertainties also follow a specific formula. The very good agreement of the present results with HITRAN2012 [**40**], HITRAN2008 [**39**] and Toth et al. [**13**] can be seen in the mean ratios and their standard deviations (in parentheses) for line intensities: Present Study/Toth et al. [**13**] = 0.997(4) and Present Study/HITRAN2012 [**40**] = 1.005(13), while Present Study/HITRAN2008 [**39**] = 0.999 (8). Although Toth et al. [**13**] measured lines up to m=60 using a Voigt line shape and the unconstrained line-by-line and spectrum-by-spectrum fitting method, those intensities compare very well with the present study, as seen in **Fig. 5(c)**. The agreement between the Present Study and HITRAN2008 [**39**] is excellent for $m \leq 72$. However, the comparison of our measured intensities with HITRAN2012 reveals larger differences beginning around m = 48 and

increases with higher *m*. Good agreement is seen between PS and HITRAN 2008 and PS and Toth et al., while a discontinuity in intensities beyond P46 and R48 is seen in the HITRAN2012 values. The line intensities for high *J* transitions in HITRAN2012 are from the CDSD-296 databank [**46**], discussed in Section 4.1. Intensity comparisons with earlier measurements and with HITRAN2004 [**38**] were given in [**18**] and hence are not repeated here. Comparisons of intensities between PS with NIST [**50**], CDSD-296 [**46**], Huang [**48**] and Zak et al. [**49**] are also made but shown later in **Fig. 15** (in the section discussing the estimated total error budget). Since the calculated intensities from Polyansky et al. [**47**] are virtually identical when extended to the same *J* as Zak et al., we have not added a separate plot for PS/Polyansky et al.

Insert Fig. 5 (intensity comparisons) here

The ro-vibrational (*G*,*B*,*D, etc.*), and transition moment constants (vibrational band strength S_v, and three Herman–Wallis type parameters a_1, a_2, a_3) for five bands obtained in this study are reported in **Table 6**, along with the correlation coefficients between appropriate pairs of fitted parameters for the upper state constants needed to compute the uncertainties in line positions and intensities. The lower state rotational constants shown were constrained to values from Miller and Brown [**29**] and Miller et al. [**30**]. We remind the readers that extrapolating calculations beyond the range of measured *J* can lead to systematic deviations, as seen in **Figs. 3, 5** and **15**. Because of the larger uncertainties associated with the corresponding constants determined for the $^{13}C^{16}O_2$ and the $^{12}C^{16}O^{18}O$ bands, and also because better parameters have been determined for those isotopologues from spectra using enriched CO_2 samples [**16**,**17**] those values are not included in **Table 6**.

As stated earlier in Section 4.1, Long et al. [**27**] reported absolute $^{12}C^{16}O_2$ transition frequencies (with combined standard uncertainties as low as 6×10^{-7} cm^{-1}) measured at the National Institute of Standards and Technology [NIST] in Gaithersburg, Maryland using the frequency-stabilized cavity ring-down spectroscopy and the measured positions were listed for seven transitions between (R6-R32) for the 30013←00001 band of $^{12}C^{16}O_2$. Spectroscopic constants (G_v, B_v, D_v, and H_v) obtained by including these 7 measurements with a much larger dataset in a global fit listed in [**27**] are compared in **Table 6**.

Good agreement is seen for the G_v, B_v, and D_v while their H_v value was considerably smaller compared to **PS**. However, it has been noted that CDSD-296 [**46**] calculations reproduce accurate measurements when values by Long et al. [**27**] were combined with other CRDS and FTS data, Lin et al. [**52**] and Burkart et al. [**53**] measurements. Lin et al. [**52**] using a cavity ring-down spectrometer system developed for near-infrared measurements were able to obtain spectra with signal-to-noise ratio of 1.5×10^6:1. With spectra obtained with their apparatus, they made line shape parameters for air-broadened carbon dioxide transitions near 1.6 μm region and modeled the line shapes using the partially correlated quadratic speed dependent Nelkin-Ghatak profile (pCqSDNGP). Burkart et al. [**53**] published line positions accurate to a few parts in 10^{11} for ten transitions in the P branch of the 30013←00001and two transitions in the R branch of the 31113←01101of $^{12}C^{16}O_2$ in the 6189-6215 cm^{-1} by measuring Doppler free saturated absorption Lamp dips at sub-Pa pressures using optical feedback frequency stabilized cavity ring-down spectroscopy.

Table 6 (fit constants comes here)

In **Table 7**, we compare the vibrational band intensities, S_v, for the 30013←00001 and the 31113←01101 bands of $^{12}C^{16}O_2$ measured in the present study (columns 2 and 4) with our previous measured values at room-temperature [**18**] and also to values obtained from line-by-line fitting using the Voigt line shape profile by Toth et al. [**13**] (columns 3 and 5). Although several other studies (*e.g.*, Refs. [**12,20**] and references cited therein) reported the 30013←00001 band intensity, we have limited our comparisons to only Refs. [**13**,**18**] since Predoi-Cross et al. [**20**] have provided detailed comparisons of their measured 30013←00001 line intensities with the results of [**12**,**13**,**18**] and other earlier studies.

Table 7 (comparing band strengths comes here)

For each parameter, the values on the top row under the columns labeled Present Study are from this study, while the values in the bottom row were retrieved in our previous study [**18**] using only room-temperature data. The Herman-Wallis a_3 parameter for the 30013←00001 band was determinable only in the present study, and, as shown in **Table 6, ** a_3 parameters were not determined for any other bands. The comparisons show good agreement of the Present Study with the room-temperature measurements

by Devi et al. [**18**] and Toth et al. [**13**], providing confidence that the $^{12}C^{16}O_2$ isotopologue abundances that we applied in all 46 spectra were properly accounted for. We emphasize that the band strengths/line intensities we have retrieved for the other two isotopologues ($^{13}C^{16}O_2$ and the $^{12}C^{16}O^{18}O$) should only be considered as relative, since more accurate measurements for these bands using enriched samples of carbon dioxide were reported by Toth et al. [**16,17**].

We provide the following discussion relating to the sum of the line intensities, S_{band}, and vibrational band strength, S_v, determined from present measurements and values listed in **Tables 6** and **7**. As discussed in Section 3 (spectral retrievals and measurements), Eq. (**1**)-(**3**) were used connecting the line positions and line intensities to the ro-vibrational constants and the vibrational band intensity (S_v) and Herman–Wallis parameters (*e.g.,* a_1,a_2,a_3). The band strength, S_{band}, is defined as the sum of all the line intensities in a band. In this work S_{band} for the 30013←00001 band of $^{12}C^{16}O_2$ is 4.4959×10^{-22} cm/molecule at 296 K. Our present band strength (S_{band}) value shows excellent agreement with: (a) our previous 2007 measurements [**18**] of room temperature data (4.501×10^{-22}); (b) Toth et al. [**13**] = 4.4357×10^{-22}; (c) HITRAN2012 [**40**] = 4.5117×10^{-22}; (d) Zak et al. [**49**] = 4.5371×10^{-22}; CDSD-296 [**46**] =4.5394×10^{-22}; and, (e) Huang [**48**] =4.5399×10^{-22} at cm/molecule at 296 K.

The vibrational band intensity, S_v, is defined starting from the general expression for the intensity of a line in terms of the total transition moment squared, which in general contains all interactions, for example see Eq. (**38**) of Ref. [**54**] or Eq. (**17**) of Ref. [**55**]. Assuming no interactions, the transition moment squared can be written as the product of a rotationless (vibrational) transition moment squared times the transition moment squared, for a rigid rotor (Hönl-London factors). Also assuming the product approximation for the total internal partition, *i.e.*, $Q_{tot} = Q_{vib}*Q_{rot}$, the line intensity expression can be written as a vibrational part times a rotational part. S_v is defined by the vibrational part;

$$S_v = \frac{8\pi^3}{3hc}\nu_{v'\leftarrow v''}\left(\frac{1-e^{-E_{v''}/kT}}{Q_v}\right)|R_{v'\leftarrow v''}|^2 \qquad (7)$$

where, h is Planck's constant, c is the speed of light, $\omega_{v'\leftarrow v''}$ is the vibrational band center, $E_{v''}$ is the lower state vibrational energy, k is the Boltzmann constant (cm^{-1}/K), T the temperature in Kelvin, Q_v is

the vibrational partition sum, and $|R_{v' \leftarrow v''}|^2$ is the vibrational transition moment squared. Furthermore, if the line intensity expression is summed over all lines of a band, a sum rule can be applied reducing the rotational part to 1 giving $S_v = S_{band}$. Note, this is only for the case of no vibration-rotation interactions. Interested readers can obtain more details in Ref. [**55**].

When there are vibration-rotation interactions, the line intensity formula is generally augmented with the Herman-Wallis factor, which defines the departure of line intensities from rigid-rotor behavior (see Eq. (2)). In such cases S_v does not equal S_{band}. The difference between the two can be used as a proxy to the strength of the vibration-rotation interactions. For most parallel bands the differences are only a few percent. In the present study, the ratio of the integrated band strength, S_{band}, to the vibrational band intensity, S_v, is 1.02, indicating a small vibration-rotation interaction for this band. When the vibration-rotation interactions are strong, significant differences between S_{band} and S_v will be observed, for examples, see Rinsland et al. [**56**].

4.3. Lorentz air- and self-broadening

Although a multispectrum fitting method was applied to fit all the 46 spectra simultaneously, and line positions and line intensities were retrieved using constraints, the air- and self-broadened half-width coefficients, pressure-shift coefficients and their temperature dependences were adjusted individually for each measured transition. The speed dependence parameter was also measured for the strong and medium strength transitions (only for the 30013←00001 band). The measured air- and self-broadened Lorentz half-width coefficients, pressure-shift coefficients, and their corresponding temperature dependences are listed in the **Supplemental File**. The majority of these were retrieved for the strong cold band (30013←00001) of $^{12}C^{16}O_2$ and its first hot-band, 31113←01101. Similar parameters were measured for a smaller number of transitions in the 40014←10002 band of $^{12}C^{16}O_2$ and the 30013←00001 band of $^{13}C^{16}O_2$, while only a very few self-width and self-shift coefficients were obtained for the 40013←10001 band of $^{12}C^{16}O_2$ and the 30013←00001 band of $^{12}C^{16}O^{18}O$. Temperature dependences for half-width, pressure-shift and relaxation matrix element coefficients were determined only for the 30013←00001 band of $^{12}C^{16}O_2$ (See the **Supplemental File**).

The measured air- and self-broadened half-width coefficients from present study for the 30013←00001 band are plotted as a function of m ($m = -J''$ for P branch lines and $J''+1$ for R-branch lines) in **Fig. 6**.

Unlike the line positions and intensities, the Lorentz half-width coefficients were not constrained in the fits to follow a smooth curve as a function of *m*. Even so, the half-width coefficients for both broadening gases vary rather smoothly with *m* for both self-broadening and air-broadening with a few exceptions at high-*J* quantum numbers (see **Fig. 6** and the **Supplemental file**).

Larcher et al. [**32**] published room-temperature self-broadened half-with coefficients for four transitions (P38, R10, R12, R20) in the 30013←00001 band of $^{12}C^{16}O_2$ using various line shape models, including the Hartmann-Tran Profile (HTP). The line shape model in [**32**] included collision-induced velocity changes and speed dependence. Because of the differences in line shape models employed in [**32**] from present study, no direct comparison with those measurements are made here. Included in **Fig. 6** are the predicted self- and air-broadened Lorentz half-width coefficients for the 30013←00001 band of $^{12}C^{16}O_2$ published by Gamache and Lamouroux [**57**]. These values show excellent agreement with other measured and theoretical values.

Insert Fig. 6 (widths here)

In the top panel **Fig. 6(a)** the measured self- and air-broadened half-width coefficients from Toth et al. [**14,15**], HITRAN2012 [**40**], the predicted values by Gamache and Lamouroux [**57**] and the measured air-broadened half-width coefficients from Predoi-Cross et al. [**24**] are plotted as a function of *m*. Ratios of half-width coefficients for each transition (present study/Toth et al. [**14,15**], present study/HITRAN2012 [**40**] and present study/Predoi-Cross et al. [**24**]) are plotted in **Fig. 6(b)**. The means and the standard deviations of these ratios are given in the legend of panel **6(b)**. The largest differences between measurements are for self-width coefficients from the present study and Toth et al. [**14**]. These large differences are attributed to the different analysis techniques and the line shape models employed in the two studies. In **Fig. 6(c)** the ratios of self- to air-broadened half-width coefficients for each transition in the present study, Toth et al. [**14**] and HITRAN2012 [**40**] are plotted vs. *m*. These ratios vary significantly with *m*, ranging from ~1.05 to ~1.35. The form of each of the three ratio plots results from the rapid decrease of self-broadened half-width coefficients with increasing $|m|$ compared to the slower variations of air-broadened half-width coefficients over the same range of $|m|$ (see **6(a)**). All three sets of ratios plotted in **6(c)** agree to within their mutual statistical uncertainties; the means and

standard deviations given in the legend of panel **6(c)** indicate the level of agreement among the three data sets.

4.4. Temperature-dependence exponents of Lorentz half-width coefficients (n_1 and n_2)

For remote sensing applications, both temperature and pressure dependence of half-width coefficients are required on a line-by-line basis. In determining the temperature dependence exponents for the Lorentz air- and self-broadened half-width coefficients, n_1 and n_2, we have employed the power law relationship given in **Eq. (4)** by simultaneously fitting all the air-broadened and self-broadened spectra recorded at all sample temperatures and pressures [see **Table 2**]. The first measurements of the temperature dependence exponents of air- and self-broadening for the 30013←00001 (and the 30012←00001) band of $^{12}C^{16}O_2$ were reported by Predoi-Cross et al. [**24,25**], who analyzed a large number of high resolution FTS spectra using the multispectrum algorithm, but the sets of air-broadened and self-broadened CO_2 spectra were analyzed separately. In those studies, the measured half-width coefficients and temperature dependence exponents were also modeled using semiclassical calculations based upon the Robert-Bonamy formalism. In the present study we have reinvestigated the 30013←00001 band by fitting a different set of experimental data obtained by two distinct FTS and combining both the self- and air-broadened spectra in a single global least squares fit, from which we retrieved both n_1 and n_2 simultaneously. Values obtained from the two studies are compared in **Fig. 7.**

Insert Fig. 7 (widths temp dependence) here

The measured values for n_1 and n_2 are plotted vs. m in **Fig. 7**. The values from present study are displayed in the upper panel **(a),** the corresponding values from Predoi-Cross et al. [**24,25**] in the middle panel **(b)** and, the predicted values [**57**] in the bottom panel **(c).** Although the range in n_1 and n_2 are generally close, there is less scatter in the results of the present study plotted in **Fig. 7(a)**. The crossings of the n_1 and n_2 vs. m graphs near $|m| = 20$ are more obvious in **7(a)** than in **7(b)**. Theoretical modeling by Gamache and Lamouroux [**57**] shows similar patterns in the m-dependences of the temperature dependence exponents for the CO_2 and air broadening. The horizontal black dashed line in all three panels corresponds to $n = 0.75$, which is close to the average value of the air-broadening temperature dependence exponents for CO_2 transitions in recent editions of the HITRAN database [**38-40**].

4.5. Air- and self- pressure shift coefficients and their temperature dependences

The measured air- and self- pressure-shift coefficients, δ^0(air) and δ^0(self), in units of cm^{-1} atm^{-1} at 296 K for the 30013←00001 band from the Present Study are plotted as a function of *m* in **Fig. 8**, along with the shift values from other recent studies [**14**, **15**, **24**] and from HITRAN2012 [**40**]. The increased scatter observed in the Present Study results at higher |*m*| values (|*m*| > 30), particularly for the air-pressure-shift coefficients, is because at these high-|*m*| (or *J*) values, the absorption lines are weaker especially when the sample temperatures are low. Also, due to the smaller optical path used for the low-temperature spectra and the low mixing ratios used for the air-broadened spectra (see **Table 3**) the number of transitions measurable in air-broadened spectra is less than for self-broadening. The general qualitative nature of variations of the pressure-shift coefficients vs. *m* is similar for both broadening gases up to |*m*| = ~20 in the R-branch and |*m*| = ~30 in the P-branch. Beyond that the self-shift coefficients steadily increase in magnitude with |*m*| while the air- pressure-shift coefficients show much smaller changes with |*m*|. The self-shift coefficients are systematically larger (more negative) than the corresponding air-shift coefficients for the same transitions. The same behavior has been observed in our previous room-temperature study of this band [**18**] and in the measurements from other studies whose results are shown in Refs. [**14, 15**, **24**]. Some differences among the measured shifts plotted in the figure for the same broadening gas are expected due to the inclusion (or not) of line mixing in the analysis. We note that the Present Study shift results shown in **Fig. 8** are in excellent agreement with the results of our previous room temperature study [**18**], which included line mixing.

Insert Fig. 8 pressure shifts here

Applying the linear temperature dependence law in **Eq. (6)**, the temperature dependence coefficients δ'(air) and δ'(self) (cm^{-1} atm^{-1} K^{-1}) were retrieved directly from the multispectrum fit. The measured δ'(air) and δ'(self) plotted vs. *m* are shown in **Fig. 9**.

Insert Fig. 9 (temp-dependence of shifts here)

The measured δ′, temperature dependences of pressure-shift coefficients (cm^{-1} atm^{-1} at 296 K) for the 30013←00001 band of $^{12}C^{16}O_2$ from the present study are plotted vs. *m* in **Fig. 9(a)** and the

corresponding values measured by Predoi-Cross et al. [**24,25**] are similarly plotted in **Fig. 9(b)**. It is puzzling to see that the range in magnitude and some signs of the temperature dependence coefficients are different in the two sets of measurements, although identical expressions (**Eq. (6)**) were used in both studies. The horizontal dashed lines in panels **(a)** and **(b)** represent zero value for the temperature dependence coefficients. It is also seen in **(a)** that for δ'(self) in the Present Study, the values for $|m|$ near 50 to ~$|m|$ =30 are positive (up to ~ $+0.25\times10^{-4}$ cm^{-1} atm^{-1} K^{-1}), and δ′ (self) gradually decreases with decreasing $|m|$ until its value reaches *zero* and continues to decrease (become more negative) until its value reaches ~ -0.3×10^{-4} cm^{-1} atm^{-1} K^{-1} near the band center. On the contrary, the temperature dependence coefficient for air-shifts, δ'(air), stays positive (except for a couple of outliers near the high-J P and R lines) but slowly varies with $|m|$, ranging in value between $+0.1\times10^{-4}$ and $+0.3\times10^{-4}$ cm^{-1} atm^{-1} K^{-1}. The overall range of our measured δ' for both broadening gases is approximately $\pm0.3\times10^{-4}$ cm^{-1} atm^{-1} K^{-1}.

The results for δ'(self) and δ'(air) by Predoi-Cross et al. [**24,25**] shown in **Fig. 9(b)** are from two separate studies involving different sets of spectra. Although non-Voigt line shape profiles with speed dependence was applied in both analysis, the self-broadened spectra [**25**] were analyzed using a dispersion profile to account for line mixing compared to line mixing with the off-diagonal relaxation matrix elements applied for the air broadening [**24**]. In both of those studies δ' showed wide variations from one m to another (especially for self-shifts), and the values had a much larger range compared to present study. There were also differences in sign with respect to the present measurements; δ'(self) in [**25**] were all positive and varied from *zero* to nearly $+2.0\times10^{-4}$ cm^{-1} atm^{-1} K^{-1} while δ'(air) [**24**] were all negative with values ranging from *zero* to nearly -8.0×10^{-5} cm^{-1} atm^{-1} K^{-1}. At this time we are not able to provide any explanations for the large observed differences between the two sets of temperature-dependence measurements of pressure-shift coefficients shown in **Fig. 9 (a)** and **(b)**, especially since the corresponding pressure- shift coefficients from the Present Study and Refs. [**24,25**] are in agreement within their respective measurement uncertainties. However, the reason for these large differences could be that the analysis in [**24**] was performed using a different spectrum fitting software and fitting different spectra.

4.6. Off-diagonal relaxation matrix element coefficients and speed dependence

It is well-known that a conventional Voigt line shape is not adequate to fit high pressure CO_2 spectra within the noise levels as seen in these spectra. In the present study, as higher pressure spectra were added to the fit, the fit residuals characteristic of line mixing were observed indicating that line mixing was required to fit the spectra to their noise levels. Line mixing via off-diagonal relaxation matrix element coefficients (W_{ij}) in cm^{-1} atm^{-1} at 296 K [**35**] between the nearest neighbor transition pairs were included systematically, for a few transition pairs at a time, in both the P and R branches, and for both CO_2-air and CO_2-CO_2 mixing, until no significant fit residuals above the noise level were apparent. Temperature dependence exponents of the off-diagonal matrix element coefficients could be measured for transitions in the strongest parts of the P and R branches for the 30013←00001 band. The temperature dependence exponents for the remaining CO_2-CO_2 and CO_2-air line-mixed pairs were fixed to a default value of 0.75 (a value comparable to the average temperature dependence exponents of the Lorentz half-width coefficients). We were not able to measure the temperature dependence exponents for the very low-*J* and high-*J* transitions in the P and R branches, and the reason for this is not clear. It may be associated with not having the optimum optical densities in the spectra used in the fittings, model deficiencies, insufficient range of gas mixture temperatures, or the combination of all of the above. The measured relaxation matrix element coefficients for CO_2-CO_2 and CO_2-air mixing (W_{ij}) in cm^{-1} atm^{-1} at 296 K, as well as their measured temperature dependence exponents, are listed in **Table 8**. Although we used a different approach to implement relaxation matrix element coefficients for CO_2-CO_2 and CO_2-air in the present analysis considering only the nearest neighbor transition pairs, Lamouroux et al. ([**58**] and other references therein) have reported updated database including software for line-mixing in CO_2 spectra and their test using laboratory spectra in the 1.5–2.3 μm region.

Table 9 comes here

The off-diagonal relaxation matrix element coefficients between the nearest neighbor pairs were measured from P2 & P4 to P48 & P50 and from R0 & R2 to R46 & R48 for CO_2-CO_2 and P2 & P4 to P36 & P38 and R0 & R2 to R40 & R42 for CO_2-air. All other (nearest neighbor) relaxation matrix element coefficients were fixed to a default value of 0.004 cm^{-1} atm^{-1} at 296 K (for both broadening gases) and for a few additional pairs of transitions (up to J''=60) to be consistent with the J_{max} for which Lorentz half-width coefficients were measured. This procedure was adopted since it is not possible to obtain reliable values of the relaxation matrix element coefficients when the absorption at higher *J*

becomes weaker at low temperatures. A power-law expression similar to **Eq. (4)** for the temperature dependence exponents of the Lorentz half-width coefficients was also used for the temperature dependence exponents for the relaxation matrix element coefficients. As mentioned earlier, the temperature dependence exponents could be determined for only a few pairs of transitions between $|m|$ = 6 and 22. The values of these line mixing temperature dependence exponents ranged between 0.67 and 1.03 and showed no systematic variations with $|m|$ or J, and hence all other unmeasured values were fixed to the default average value of 0.75.

The measured relaxation matrix element coefficients, (W_{ij}) in cm^{-1} atm^{-1} at 296 K, listed in **Table 8** for both CO_2-CO_2 and CO_2-air are plotted in **Fig. 10(a)** as a function of the rotational quantum number index m. The measured relaxation matrix element coefficients range from ~0.002 to 0.023 cm^{-1} atm^{-1} at 296 K for CO_2-air while for CO_2-CO_2 the values range between ~0.005 and 0.033 cm^{-1} atm^{-1} at 296 K. For CO_2-air the relaxation matrix element coefficients measured in the P and R branches are close (but not the same value) for transitions with similar $|m|$. In the case of CO_2-CO_2, the relaxation matrix element coefficients in the R branch are larger than those for corresponding $|m|$ in the P branch, and more measurements to higher J are made in the R branch than in the P branch. For comparisons, we have also plotted the relaxation matrix element coefficients measured in our previous study of 30013←00001 band [**18**] from room-temperature spectra; the two sets of values agree well even though the present study included both room- and low-temperature spectra. Since the number of measured temperature dependence exponents of the relaxation matrix element coefficients was limited we did not plot their values, which are listed in **Table 8**.

The line shape profile in the present study assumes a quadratic speed dependence on molecular collision velocity. The speed dependence parameter was measured for the strong and medium strength transitions in the 30013←00001band of $^{12}C^{16}O_2$. The expression given in **Eq. (8)** to describe the Lorentz width as a function of velocity was used in several of our previous studies [*e.g.*, **18**, **19**] and was applied to model the speed dependence for transitions with J up to 46.

$$b_L^0(v) = b_L^0(v_m)\left\{1 + S\left[\left(\frac{v}{v_p}\right)^2 - c\right]\right\} \qquad (8)$$

In the above expression, v is the speed of the molecular collision, v_m is the mean speed of the molecular collision, v_p is the most probable speed of the collision, and S is the speed dependence parameter (SD) reported in this study. c is a constant and its value is taken to be 1.5 so that the Lorentz width will be the same when S=0 as that usually used in the Lorentz equation when speed dependence is neglected. When this expression is placed into the Voigt expression and integrated over all velocities of collision, the resulting real (K_s) and imaginary (L_s) expressions for the line shape becomes those of **Eq. (9)**.

$$K_s(x,y,S) = \frac{2}{\pi}\int_{-\infty}^{\infty} e^{-v^2}\, v \tan^{-1}\left\{\left[\frac{v+x}{y(S\{v^2-c\}+1)}\right]^2\right\} dv \qquad (\mathbf{9a})$$

$$L_s(x,y,S) = \frac{1}{\pi}\int_{-\infty}^{\infty} e^{-v^2}\, v \ln\left\{\left[\frac{v+x}{y(S\{v^2-c\}+1)}\right]^2 + 1\right\} dv \qquad (\mathbf{9b})$$

For transitions for which speed dependence was not measured, that parameter's values were fixed to 0.1 for P42-P62 and 0.07 for R46-R58 (see the last two columns in the **Supplemental file**). The measured values are plotted in **Fig. 10(b)** along with those from our earlier study [**18**].

Insert Fig. 10 (line-mixing &speed-dep)

It is clear that the results obtained in the present study are about 20-25% smaller compared to [**18**] for all P-branch transitions and for R-branch transitions between m = 1 and 21. This study included a large number of low temperature spectra, but our analysis assumed that the speed dependence is independent of the broadening gas (CO_2 and air in this case) and also independent of the gas sample temperatures. These assumptions could cause some of the large discrepancy between the present measurements and [**18**]. Lisak et al. [**59**] recently published theoretical prediction for the temperature dependence of the quadratic speed dependence parameter. Future analysis could include the model of Lisak et al. as an appropriate physical constraint on the speed-dependent parameter.

We note that because the present study included a number of low-temperature spectra, and temperature dependence exponents of the relaxation matrix element coefficients were retrieved for transitions with

J''= 6 to 24 while the previous study [**18**] included only room-temperature spectra and assumed a constant temperature dependence exponent of 0.75 for all line mixing coefficients.

5. Uncertainties in some measured parameters

5.1. Lorentz half-width coefficients

In simulating the spectrum of a gas/molecular band, it is not the uncertainties in the Lorentz half-width, pressure-shift or the relaxation matrix elements of the transitions that are important, but the uncertainties in those line parameters at the temperature at which the spectrum is to be simulated. As discussed in [**24**] when one uses a half-width coefficient at T=296 K and its temperature dependence exponent (n) from a database such as the HITRAN, it is normally assumed that the half-width coefficients near 296 K are the best determined values, and the uncertainty in the temperature dependence exponent (n) increases the uncertainty in half-width coefficient as the temperature gets farther from 296 K. This is not always the case as shown in the following discussions.

As examples, in **Fig. 11**, we have plotted the formal (internal statistical) uncertainty in the measured Lorentz half-width coefficient (cm^{-1} atm^{-1}) vs. the gas sample temperatures (K) for a set of air- and self-broadened transitions for the 30013←00001 band. We have chosen P4, P18, R18 and R42 to represent low J-, medium J- and high J-transitions. Plots are shown for uncertainties in both air- and self-width coefficients vs. sample gas temperatures.

For the P(4) (air- and self-broadened widths) the minimum uncertainty occurs near ~ 210 K, for the P(18) air- and self-broadened half-width coefficients, the uncertainty minima are near 225 K, and for the R(42) air-broadening the minimum uncertainty in half-width coefficients is near 240 K. The uncertainties in half-width coefficients for the low J lines are relatively constant over the range of the spectra in the fit (170 –296 K). For higher-J lines, as the intensities of the transitions become weak at

Insert Fig. 11 (unc-vs-temp) here

low temperatures, the fit does not adequately determine the half-width coefficients at those temperatures, and the temperature region in which the half-width coefficients are best measured narrows to only the higher temperatures of the fitted spectra. The trend toward lower uncertainties at higher temperature for higher rotational quantum numbers is clear (curves labeled R42 in the figure) as

is the trend toward lower uncertainties at low temperature in the strongest lines for the low-to-intermediate *J* values (curves labeled P4 in the figure).

5.2. Uncertainties in pressure-shift coefficients

The uncertainties of air- and self-broadened pressure-shift coefficients as a function of gas sample temperature for the same set of transitions (P4, P18, R18 and R42) in the 30013←00001 band are plotted in **Fig. 12**. Similar to the uncertainty vs. gas sample temperature for the Lorentz half-width coefficients, the uncertainties in the pressure-shift coefficients also tend to be smallest around the middle of the temperature range of the fitted spectra (170 K-296 K) and increase more towards the higher temperatures. For the high-*J* transitions the deviations from the minima increase rapidly as the sample temperatures are beyond the measurement range (especially for air-broadening). The uncertainties derived from the multispectrum fits for both the Lorentz half-width and pressure shift coefficients are smaller than the real uncertainties because of the large number of spectra included in the least squares fittings that reduce small uncertainties from the noise levels in the spectra (because of the high S/N). The remaining systematic uncertainties dominating the actual uncertainties are due to unknown errors in wavenumber calibration uncertainty of the spectra, the knowledge of the physical conditions of the spectra, the spectral line shape used and other modeling of the spectral line parameters. Line mixing influences the pressure-shifts of the transitions in addition to affecting other line parameters such as intensities and speed dependence; each of which has some small role in the overall solution. The general shapes of the uncertainty curves with temperature plotted in both **Figs. 11** and **12** are independent of the systematic effects, and the relative uncertainty from temperature to temperature is close to that plotted in **Figs. 11** and **12**.

Insert Fig. 12 (unc temp-dep shift) here

5.3. Uncertainties in the measured relaxation matrix elements

The uncertainty in the measured relaxation matrix element coefficients (cm^{-1} atm^{-1}) vs. gas sample temperature (K) is shown in **Fig. 13** for two transitions pairs P12-P14 (self- and air-) and R12-R14 (self- and air-). The plots show that the uncertainties in the relaxation matrix element coefficients increase more rapidly towards lower temperatures (~ below 190 K) compared to the slow increase toward higher temperature. Similar to the P18 and R18 curves in the uncertainty plots for the half-width

and pressure-shift coefficients (**Figs. 11** and **12**), the minimum uncertainty for the measured relaxation matrix element coefficients for CO_2-air at medium J'' also occurs near the middle of the fitted temperature range (170 K-296 K) (though relaxation matrix element coefficients are reported at 296 K), but for the CO_2-CO_2 mixing the minimum uncertainty is shifted to ~280 K, near room temperature.

Insert Fig. 13 unc-line-mix-vs-temp here

6. Estimated total error budget

Examples of the measured line parameters resulting from the present study are listed in **Table 5** for selected 30013←00001 transitions along with the one sigma internal statistical error associated with each measured line parameter. These uncertainties are solely based upon the formal uncertainties from the least squares fits and do not include errors arising from unknown sources. Because of the large range in pressures, volume mixing ratios and temperatures of both pure samples and air-broadened CO_2 samples, and by fitting all the spectra simultaneously the random errors are greatly minimized. The absolute uncertainties in the retrieved parameters due to unknown sources are associated with experimental physical conditions of the data such as those related to the knowledge of the absorption path lengths, gas sample temperatures, pressures, and calibration uncertainties. The absolute accuracies in the listed parameters due to unknown sources of errors are estimated conservatively to be ~ ±1.0% for line intensities, 2-3% for Lorentz half-width coefficients, and 5–10% for pressure-shift coefficients and the temperature dependences of half-width and pressure-shift coefficients. The absolute accuracies in the off-diagonal relaxation matrix element coefficients and their temperature dependence exponents and speed dependence parameters are more difficult to estimate and could range ±10–20% of the measured values, depending upon the measurement quality of the transition involved.

To compute the absolute accuracies in our measured line intensities we have estimated the various contributions due to systematic error sources: (a) 0.3-0.4% in the knowledge of path lengths, (b) 0.1-0.2% in pressure readings, (c) 0.1-0.2% in temperature readings, and (d) 0.1-0.2% background polynomial fits, field of view corrections, residual phase errors, zero level determinations and, some undetermined contribution due to model deficiencies in our analysis. The global standard deviation of weighted observed minus calculated fit residuals are only 0.056%, thus eliminating almost all random errors to within the noise levels of the fitted spectra. The maximum contribution due to sample pressure

uncertainties corresponds to smallest gas pressure; the uncertainties in higher pressures are not very significant. In any experimental setup involving absorption cells, pressure and temperature gauges, outgassing/desorption/absorption of gas samples, determination of isotopologue abundances, systematic errors are difficult to eliminate. We have taken the best care possible in determining the various measured quantities and applied the best available tool to analyze the data.

Calculations of new line intensities (and positions) for CO_2 including the 1.6 μm region have been reported recently [**46-49**]. For a comprehensive understanding of the changes in the evolution of the CO_2 line intensities (including the 30013–00001 band) listed in HITRAN database [**38-40**], and to compare our results with recent measurements [**50**] and the most recent calculations [**46-49**], we include two figures [**Figs. 14** and **15**]. In **Fig. 14(a)** comparison of line position differences between HITRAN2012 [**40**] and CDSD-296 [**46**] vs. *m* and in **14(b)** percent intensity differences between HITRAN2012 and CDSD-296 [**46**] vs. *m* are shown. In both **(a)** and **(b)** the values corresponding to higher *m* (=50 and beyond shown by **solid red circles**) are predicted values from various sources (see **Section 4**). As seen in **Fig. 14**, the position differences between HITRAN2012 and CDSD-296 lie between +0.000027 and +0.000046 cm^{-1} for P46–R48 and, beyond that the differences are within ±0.003 cm^{-1}. For the same range in *J*, the % intensity differences between HITRAN2012 and CDSD-296 are small and vary approximately from -0.8 to +0.4 and from -0.9 to -0.6, respectively.

Insert Fig. 14 here (Comparisons between HITRAN2012 vs. CDSD-296)

Line intensities for 27 transitions (P32-P4 and R28-R50) in the 30013–00001 $^{12}C^{16}O_2$ band were measured [**50**] at the National Institute of Standards and Technology (NIST) using the frequency-stabilized cavity ring-down spectroscopy technique [FS-CRDS]. Those experimental measurements were reported in a joint experimental and theoretical *ab initio* calculations published by Polyansky et al. [**47**]. The details of the experimental measurements from NIST are available in [**47**] where the measured line intensities (isotopologue abundance of 0.984599) are listed in **Table 1** of the Supplementary file [**47**]. For comparisons shown in **Fig. 15**, the NIST intensities, given at an isotopologue abundance of 0.984599, were scaled to the natural isotopologue abundance of 0.9842. A few of those experimental details are repeated here in comparing the line intensities between NIST measurements and the present study to understand the reason for the intensity differences. The 27 line

intensities in [**50**] were measured line-by-line using gas samples of known molar fraction of CO_2 in air with values that were referenced to gravimetrically-prepared primary standard mixtures. To prevent exchange of CO_2 with the surface of the absorption chamber, the sample was continuously introduced into the absorption chamber. The sample pressures were in the 50–150 Torr range, and each line was fit with the sum of a linear baseline and multiple quadratic speed-dependent Nelkin-Ghatak profile. Recently, Zak et al. [**49**] reported *ab initio* calculated intensities for P92–R92 transitions for the 30013←00001 band. The comparisons of present line intensities to the new measurements [**50**] and *ab initio* calculated values for P74-R72 [**47**-**49**] and calculated CDSD-296 line parameters [**46**] are shown in **Fig. 15 (a-f)**.

In **Fig. 15**, the ratios of line intensities between **PS** and [**47,49,50**] vs. *m* are plotted. The line intensities [**47**,**50**] plotted were scaled to match the natural isotopologue abundance of $^{12}C^{16}O_2$ in HITRAN [**38**-**40**]. The following mean ratios of line intensities with standard deviations are obtained: Polyansky et al. [**47**]/Zak et al. [**49**]=1.0012(2), PS/Zak et al. [**49**]=0.9960(79) and NIST/Zak et al. =1.0049(23). We find that line intensities from present study are about −1.3% lower than the NIST measurements, but agree reasonably well considering the ~1% absolute error estimated in this study. Note that the mean and standard deviation of the intensity ratios between the best laboratory measurements [NIST] and the latest *ab initio* [**49**] calculated intensities for the 27 transitions in common are 1.0049(23); while a similar ratio between present measured intensities and the *ab initio* [**49**] calculated intensities for the P74-R72 transitions is 0.9960(79). Line mixing (off-diagonal relaxation matrix formalism) included in the **PS** could influence line intensities, although its magnitude is not quantified at this time. The very good agreement (0.996±0.008) in line intensities between **PS** and the *ab initio* calculated intensities [**49**] is very encouraging.

In addition to plotting the intensity ratios discussed above, we have shown several other comparisons in various panels (b)-(f) of **Fig. 15**. In (**b**) Line position differences PS-CDSD-296 are shown; in (**c**) ratios of line intensities between PS/CDSD-296, PS/Huang [**48**], CDSD-296/Huang; and Zak et al./CDSD-296 are plotted. It is interesting to see that the curvature observed in the intensity ratios between PS/Zak et al. in panel (**a**) and between PS/CDSD-296 seen in panel (**c**) are also seen in the plots showing the intensity ratios between other *ab initio* [**48**,**49**] and calculated [**46**] intensities, though to a lesser degree; (**d**) Ratios of Lorentz air- and self-broadened half-width coefficients between PS and CDSD-296; (**e**)

temperature dependence exponents of Lorentz air-broadened half-width coefficients from PS and CDSD-296; and, (**f**) air- pressure-shift coefficients from PS and CDSD-296. In addition to the good agreement seen between present measurements and CDSD-296 for line positions, intensities and Lorentz half-width coefficients as shown in panels (**b**)-(**d**) for P56-R54 transitions, it is very encouraging to see also the excellent agreements in the temperature dependence exponents for air-broadened half-width coefficients and air- pressure-shift coefficients obtained from **PS** and the CDSD-296.

Insert Fig. 15 here (Comparisons of several parameters)

As an additional check of our fitting results, we compared synthetic spectra computed from our final multispectrum fit against two air-broadened CO_2 spectra not used in our analysis. They were recorded using a White cell whose path length was 32.54 m. The gas sample temperatures were 295.3 and 293.2 K, respectively. Their total sample pressures and CO_2 volume mixing ratios were 742.08 Torr and 0.090341, 550.67 Torr and 0.090344, respectively (see **Table 3**). We found that all the retrieved parameters from the present work reproduced the two observed spectra with their fitting residuals within less than 0.2% when floating only the zero level, FTS residual phase errors and the background parameters. We note that our fit results represent a self-consistent set of parameters, and should be used as a complete set. For example, as a second test, we scaled our intensities by a factor of 1.0122 (a preliminary, but close estimate to the difference between PS and NIST) in our forward model described above and carried out forward model calculations for our measured 46 laboratory spectra included in our fit. It was found that fixing intensities to NIST values resulted in an unacceptable minimum with systematic residuals up to 0.7%, thus indicating that the NIST intensities are not compatible with the line shape parameters determined in the present work. In the future, we will investigate if a different set of line shape parameters are retrieved when the intensities are fixed to the NIST values and other parameters are floated in the new multispectrum fits.

7. Conclusions

In the present study, we were able to fit all of the 46 experimental spectra to their noise levels with only temperature dependent nearest neighbor relaxation matrix element coefficients and other standard, line-by-line parameters. Including the off-diagonal relaxation matrix element coefficients and speed

dependence parameters in the fits, we were able to determine the line shape parameters better than any previous studies so far for this band. It is important that for accurate simulation of the spectrum that a self-consistent set of line parameters be used. Our measured line parameters are based upon a set of 46 high resolution high S/N spectra covering a wide range of pressures, temperatures and widely varying absorption paths and were fitted simultaneously using a unique, well proven multispectrum fitting program. From our analysis we have provided a consistent set of spectral line parameters, such as positions, intensities, Lorentz air- and self-broadened half-width coefficients and their temperature dependence exponents, air- and self- pressure-shift coefficients and their temperature dependence coefficients, off-diagonal relaxation matrix element coefficients and their temperature dependence exponents, and the speed dependence parameters. All these parameters were measured for transitions in the 30013←00001 band. There are more than half a dozen bands in addition to the 30013←00001 band producing weak absorption features in the fitted region. Except for the first hot band 31113←00001, all other bands are weak. However, fits to the weaker bands were needed to determine accurate parameters for the 30013←00001 band. Only positions and intensities and in a few cases self-broadened half-widths and pressure-shift coefficients were also measured in a few of these weaker bands. In principle, all bands exhibit non-Voigt line shapes provided sufficient optical densities are available, such as in atmospheric remote sensing or cavity ring down spectra.

It is important that a standard line shape model with line mixing be used to establish inter-laboratory comparisons of various spectral line parameters and spectral database standardization. The parameterization presented in this study should work well for retrievals of CO_2 in the earth's atmospheric conditions. However, it is not clear whether this parameterization would work equally well for the Venusian atmosphere.

Although the present measurements included absorption features arising from several weaker bands, most of the temperature dependences of line shapes could only be determined for the strongest 30013←00001 band of $^{12}C^{16}O_2$. Ideally, one should be able to retrieve all those parameters for all of the bands in the fitted region. For the future, similar studies could be pursued to include all the bands producing observable absorptions in the fitted interval. This could only be achieved by carefully selecting data by Cavity Ring Down and Photo-acoustic techniques and analyzed using a multispectrum fitting technique that includes new line shape models [*e.g.*, **52**,**59,60]**. We recall that recently Lisak et

al. [**59**] have published theoretical predictions for the temperature dependence of the quadratic speed dependent parameter.

Our new measurements of the temperature dependences for the air- and self-broadened Lorentz widths, pressure-shifts, and line mixing parameters via the off-diagonal relaxation matrix element coefficients along with speed dependence offer unprecedented precision for the 1.6 μm region over the range of conditions encountered in Earth's atmosphere. Our database will be used to generate absorption coefficients for use within the OCO-2 retrieval algorithm. When simulating the spectrum of CO_2, the best fits to laboratory data are achieved *only* when using the complete, consistent set of line parameters; the full accuracy would be reduced if our present line parameters were used employing another line shape/line mixing model or with a mixture of parameters from our study with other studies. We are analyzing a similar set of high-quality room- and low-temperature spectra for the 2-μm region of CO_2 using a similar analysis tool.

Acknowledgments

Part of the material related to Kitt Peak measurements presented in this investigation was based upon our previous work supported by the National Science Foundation under Grant # ATM-0338475 to the College of William and Mary. The recent study involving the low-temperature measurements was supported by contracts to the College of William and Mary for the OCO-2 mission through JPL. The research at the Jet Propulsion laboratory (JPL), California Institute of Technology, Connecticut College and NASA Langley Research Center was performed under contracts and cooperative agreements with the National Aeronautics and Space Administration. One of the authors, RRG, was supported by the National Science Foundation through Grant # AGS-1156862.

Table titles

1. Summary of recent line shape measurements[a] (number and quantum number range) for the 30013←–00001 band of $^{12}C^{16}O_2$.

2. Experimental setups and physical conditions of analyzed CO_2 spectra.
3. Summary of experimental conditions of the CO_2 spectra analyzed in this work.
4. Measured line parameters and number of CO_2 measurements.
5. A sample of measured line parameters for the P40-R40 transitions in the 30013←–00001 band of $^{12}C^{16}O_2$.
6. Ro-vibrational, vibrational band intensity, Herman–Wallis parameters and correlation coefficients of measured $^{12}C^{16}O_2$ bands: 6120–6280 cm^{-1}.
7. Comparison of band intensity[a] parameters for the 30013←–00001 and 31113←–01101 bands of $^{12}C^{16}O_2$.
8. Off-diagonal relaxation matrix element coefficients, W_{ij}, and their temperature dependence exponents for CO_2-CO_2 and CO_2-air mixing in the 30013←–00001 band of $^{12}C^{16}O_2$.

Figure Captions

Fig. 1. The multispectrum fit in the 1.6-μm bands of CO_2 covering the 6120-6280 cm^{-1} spectral region. All 46 observed spectra fitted simultaneously are overlaid in the bottom panel (f) with the weighted (observed minus calculated) fit residuals plotted in the top panels (a)-(e) corresponding to selected spectra grouped at different temperature ranges. Fit residuals plotted for each group are taken from the multispectrum fit of all 46 spectra, and the color of each group of residuals corresponds to their color in panel (f). The solid horizontal line at the bottom of (f) indicates the 100% absorption line. The black short vertical lines at the top of (f) correspond to positions of all absorption lines included in the multispectrum fit. (For interpretation of the reference to color in this figure legend, the reader is referred to the electronic version of this article).

Fig. 2. A short spectral interval (6220-6235 cm^{-1}) from **Fig. 1** re-plotted on an expanded wavenumber scale to show details near the band center. Colors and symbols have the same meanings as in **Fig. 1**. The minimal residuals seen overall indicate that the line shape model incorporating the line mixing (relaxation matrix elements) and speed dependence has well characterized the spectra. In this expanded plot, some small features under (P2-P6) and (R0-R2) are seen in the residuals of panels (b) and (c). Interestingly, those residual features are nearly absent for the higher and lowest temperature spectra. (For interpretation of the reference to color in this figure legend, the reader is referred to the electronic version of this article).

Fig. 3. Comparison of line position differences: Open black triangles: Present Study–HITRAN2012 [**40**]; Open inverted purple triangles: Present Study–HITRAN2004 [**38**]; Filled red stars: Present Study–HITRAN2008 [**39**]; and Open dark red circles: Present Study−Toth et al. [**13**]; Blue checker squares: Present Study–Long et al. [**27**]; **Open inverted green down triangles**: PS- Majcherova et al. [51]; Open purple diamonds: PS-CDSD-296 [**46**]. (For interpretation of the reference to color in this figure legend, the reader is referred to the electronic version of this article).

Fig. 4. Plots of two experimental spectra used in the present analysis to illustrate the strengths of the high *J* lines measured in the present study. (a) Plots from 6150-6270 cm^{-1} (b) The interval 6150-6170 cm^{-1} showing the high–*J* P lines and, (c) the 6250–6270 cm^{-1} interval showing the high–*J* R transitions. (see the text for details).

Fig. 5. (a) and (b). Line intensities in natural abundance determined in the Present Study (**solid red triangles**) for the P and R branches for the 30013←00001 band of $^{12}C^{16}O_2$ plotted as a function of m (m = -J'' for P-branch and J''+1 for R-branch lines), and compared to HITRAN2012 [**40**] line intensity values (**solid black curve**). A linear scale is used in **(a)**, while a logarithmic scale is used in **(b)**. In **(b)** both the measured line intensities (**solid red triangles**) and their uncertainties (**open red triangles**) are plotted. In **(c)** the ratios of line intensities are plotted with error bars. **Solid black triangles**: Present Study/HITRAN2012 [**40**]; **Open green stars**: Present Study/HITRAN2008 [**39**], and **Open brown diamonds**: Present Study/Toth et al. [**13**]. The larger error bars in **(c)** are dominated by the uncertainties in Toth et al. [**13**].

Fig. 6. **(a)** Measured Lorentz self- and air-broadened half-width coefficients (cm^{-1} atm^{-1} at 296 K) in the 30013←00001 band of $^{12}C^{16}O_2$ plotted as a function of m ($m = -J''$ for P-branch and J''+1 for R-branch lines). The half-width coefficients are compared to those by Toth et al. [**14,15**], HITRAN2012 [**40**], Predoi-Cross et al. [**24**] and the predicted values by Gamache and Lamouroux [**57**]. **(b)** The ratios of Present Study (PS)/Other Study half-width coefficients for the data sets plotted in **(a)**; the mean and standard deviation (in parentheses) of each ratio for the entire band is given in the legend. **(c)** The ratios of measured self- to air-broadened half-width coefficients for each transition are plotted separately for three data sets (PS, Toth et al. [**14**,**15**], and HITRAN2012 [**40**]). The means and standard deviations of these ratios are also given in the legend. In each panel, where error bars are not visible the uncertainties are smaller than the size of the symbols used.

Fig. 7. Measured temperature dependence exponents for the Lorentz air- and self-broadened half-width coefficients (n_1 and n_2, respectively) in the 30013←00001 band of $^{12}C^{16}O_2$ plotted as a function of m ($m = -J''$ for P-branch and J''+1 for R-branch lines). Upper panel: **(a)** the measured n_2 (**dark green solid circles**) and n_1 (**black solid diamonds)** from the Present Study. Middle panel: **(b)** the measured n_2 (**solid brown inverted triangles**) and n_1 (**solid blue stars**) from Refs. [**24,25**]: Bottom panel **(c)** the predicted n_2 (**solid pink triangles**) and n_1 (**solid green stars**) from Ref. [**57**]. The black horizontal dashed lines in **(a), (b)** and **(c)** correspond to the temperature dependence exponent n = 0.75. In all three panels, where the error bars are not visible, they are smaller than the symbol size. (For interpretation of the reference to color in this figure legend, the reader is referred to the electronic version of this article).

Fig. 8. Measured self- and air- pressure-shift coefficients (cm^{-1} atm^{-1} at 296 K) in the 30013←00001 band of $^{12}C^{16}O_2$ vs. m ($m = -J''$ for P-branch and $J''+1$ for R-branch lines) in the present study compared to other reported values. The symbols are **Present study** (self-broadened) = **solid red triangles**; **Present study** (air-broadened) = **solid black circles**; Toth et al. [**14**] (self-broadened) = **solid brown diamonds**; Toth et al. [**15**] (air-broadened) = **black inverted open triangle**; HITRAN2012 [**40**] (air-broadened) = **black crosses**; Predoi-Cross et al. [**24**] (air-broadened) = **solid blue stars**. Where the error bars are not visible, they are smaller than the symbol size. (For interpretation of the reference to color in this figure legend, the reader is referred to the electronic version of this article).

Fig. 9. Measured δ', temperature dependences of self- and air- pressure-shift coefficients (cm^{-1} atm^{-1} K^{-1}) in the 30013←00001 band of $^{12}C^{16}O_2$ (defined by **Eq. (6)**) vs. m ($m = -J''$ for P-branch and $J''+1$ for R-branch lines). Symbols are: upper panel **(a)** δ'(self) (**Present study**) = **dark solid green circles**; δ'(air) (**Present study**) = **solid black diamonds**; lower panel **(b)** δ'(self) (Predoi-Cross et al. [**25**]) = **solid brown triangles**; δ'(air) (Predoi-Cross et al. [**24**]) = **solid blue inverted triangles**. The dashed horizontal line in **(a)** and **(b)** corresponds to $\delta' = 0$. In each panel, where error bars are not visible, they are smaller than the size of the symbol. (For interpretation of the reference to color in this figure legend, the reader is referred to the electronic version of this article).

Fig. 10. Upper panel **(a)**: Measured off-diagonal relaxation matrix element coefficients, W_{ij}, (cm^{-1} atm^{-1}) at 296 K for CO_2-CO_2 and CO_2-air line mixing plotted vs. m ($m = -J''$ for P-branch and $J''+1$ for R-branch lines) for the 30013←00001 band of $^{12}C^{16}O_2$. **Solid dark blue diamonds**: self-mixing, Present Study; **Solid up red triangles**: self-mixing, Ref. [**18**]; Solid purple circles: air-mixing, Present Study; **Solid inverted black triangles**: air-mixing, Ref. [**18**]. Lower panel **(b)**: The measured speed dependence parameter in the P and R branches for the 30013←00001 band plotted against m. The speed dependence parameter is assumed to be independent of the broadening gas and sample temperature, and a single value is given for each transition. **Solid dark blue circles**: Present Study; **Solid red stars**: Ref. [**18**]. In both panels, where error bars are not visible, the uncertainties are smaller than the symbol.

Fig. 11. Uncertainty of self- and air-broadened Lorentz half-width coefficients (cm^{-1} atm^{-1}) plotted as a function of the gas sample temperature (K) for the 30013←00001 band of $^{12}C^{16}O_2$ illustrating that the minimum uncertainty does not always correspond to T= 296 K (where half-width coefficients are

reported). Plots are made for both self- and air-broadening for P4, P18, R18 and R42 transitions. Plots for middle *J*-transitions overlap and are not labeled individually. For the low- and mid-*J* transitions, the uncertainties do not vary much with gas temperatures, but the minimum uncertainty is in the 220-230 K range. For the high-*J* lines, the uncertainty increases rapidly below about 200 K.

Fig. 12. Uncertainty of self- and air- pressure-shift coefficients (cm^{-1} atm^{-1}) plotted as a function of the gas sample temperature (K) for 30013←00001 band of $^{12}C^{16}O_2$ illustrating that the minimum uncertainty does not always correspond to T= 296 K (where pressure shift coefficients are reported). The curves represent the uncertainties of both self- and air-shift coefficients for P4, P18, R18 and P42 transitions. Plots for middle *J*-transitions are close and are not labeled individually. The minimum uncertainty for R42 air-shifts is near 230 K while for R42 self-shifts, the minimum uncertainty occurs near 270 K.

Fig. 13. Uncertainty in the measured relaxation matrix element coefficients (cm^{-1} atm^{-1}) plotted as a function of the gas sample temperature (K) for the 30013←00001 band of $^{12}C^{16}O_2$ for self (CO_2-CO_2) and (CO_2-air) mixing. Plots are made for four line-mixed transition pairs, P12-P14 self- and air-mixing and R12-R14 self- and air-mixing (two each for CO_2-CO_2 and CO_2-air). The minimum uncertainty for CO_2-air mixing occurs at lower temperatures (220 K, 240 K) compared to CO_2-CO_2 mixing (~ 280 K).

Fig. 14. **(a)** Comparison of line position differences between HITRAN2012 [**40**] and CDSD- 296 [**46**] vs. *m*. **(b)** Percent intensity differences between HITRAN2012 and CDSD-296 vs. *m*. In (**a**) and (**b**), the CDSD-296 data points for P46-P2 and R0-R48 (**open black stars**) were calculated using the experimental values from Toth et al. [**17**] and for the higher *m* values **(solid red circles)** from Refs. [**45**,**46**] (see the text for details). (For interpretation of the reference to color in this figure legend, the reader is referred to the electronic version of this article).

Fig. 15. (**a**) Ratios of line intensities: **Red circles**: Polyansky et al. [**47**]/Zak et al. [**49**]; **Solid green stars**: PS/Zak et al.; **Dark brown triangles**: NIST/Zak et al. For the same transitions measured in the NIST study [**50**] the mean ratio PS/Zak et al. = 0.992(2). (**b**) Line position differences PS-CDSD-296; (**c**) Ratios of line intensities between PS/CDSD-296, PS/Huang [**48**], CDSD-296/Huang; and Zak et al./CDSD-296; (**d**) Ratios of Lorentz air- and self-broadened half-width coefficients between **PS** and CDSD-296; (**e**) temperature dependence exponents of Lorentz air-broadened half-width coefficients from **PS** and CDSD-296; and, (**f**) air- pressure-shift coefficients from **PS** and CDSD-296. See the text

for details. (For interpretation of the reference to color in this figure legend, the reader is referred to the electronic version of this article).

References

1. Crisp D, Atlas RM, Breon PM, Brown LR, Burrows JP, Ciais P, et al. The Orbiting carbon Observatory (OCO) mission. Adv Space Res 2004;34:700-9.

2. Crisp D, Miller CE, DeCola PL. Orbiting carbon Observatory: measuring the column averaged carbon dioxide mole fraction from space. J Appl Rem Sens 2008: http://dx.doi.org/10.1117/1.2898457.

3. Boesch H, Baker D, Connor B, Crisp D, Miller CE. Global characterization of CO_2 column retrievals from shortwave-infrared satellite observation of the Orbiting Carbon Observatory-2 mission. Remote Sens 2011;3:270-304.

4. Kuze A, Suto H, Nakajima M, Hamazaki T. Thermal and near infrared sensor for carbon observation Fourier transform spectrometer on the Greenhouse Gases Observing Satellite for greenhouse gases monitoring. Appl Opt 2009;48:6716–33, doi:10.1364/AO.48.006716 2009.

5. O'Dell CW, Connor B, Boesch H, O'Brien D, Frankenberg C, Castano R, et al. The ACOS CO_2 retrieval algorithm – Part 1: Description and validation against synthetic observations. Atmos Meas Tech 2012;5: 99–121. doi:10.5194/amt-5-99-2012,2012.

6. Crisp D, Fisher BM, O'Dell, C, Frankenberg, C, Basilio R, Boesch H, et al. The ACOS CO_2 retrieval algorithm – Part II: Global XCO_2 characterization. Atmos Meas Tech 2012;5:687-707.

7. Connor BJ, Boesch H, Toon G, Sen B, Miller C, Crisp D. Orbiting Carbon Observatory: inverse method and prospective error analysis. J Geophys Res 2008;113,D05305, doi: 0.1029/2006JD008336, 2008.

8. Miller CE, Crisp D, Decola PL, Olsen SC, Randerson JT, Michalak AM, et al. Precision requirements for space-based XCO_2 data. J Geophys Res 2007;112:D10314. http://dx.doi.org/10.1029/2006JD007659.

9. Miller CE, Brown LR, Toth RA, Benner DC, Devi VM. Spectroscopic challenges for high accuracy retrievals of atmospheric CO_2 and the Orbiting Carbon Observatory (OCO) experiment. C R Phys 2005;6:876-87.

10. Washenfelder RA, Toon GC, Blavier JFL, Yang Z, Allen NT, Wennberg PO, et al. Carbon dioxide column abundances at the Wisconsin Tall Tower site. J Geophys Res. 2006;111:D22305. http://dx.doi.org/10.1029/2006/D007154.

11. Thompson DR, Benner DC, Brown LR, Crisp D, Devi VM, Jiang Y, et al. Atmospheric validation of high accuracy CO_2 absorption coefficients for the OCO-2 mission. J Quant Spectrosc Radiat Transf 2012;113:2265-76.

12. Regalia-Jarlot L, Zenninari V, Parvitte B, Grossel A, Thomas X, Heyden P von der, et al. A complete study of the line intensities of four bands of CO_2 around 1.6 and 2.0 μm: A comparison between Fourier transform and diode laser measurements. J Quant Spectrosc Radiat Transf 2006;101:325-38.

13. Toth RA, Brown LR, Miller CE, Devi VM, Benner DC. Line strengths of $^{12}C^{16}O_2$: 4550-7000 cm^{-1}. J Mol Spectrosc. 2006;239:221-42.

14. Toth RA, Brown LR, Miller CE, Devi VM, Benner DC. Self-broadened widths and shifts of $^{12}C^{16}O_2$: 4750-7000 cm^{-1}. J Mol Spectrosc 2006;239:243-71.

15. Toth RA, Miller CE, Devi VM, Benner DC, Brown LR. Air-broadened halfwidth and pressure shift coefficients of $^{12}C^{16}O_2$ bands: 4750-7000 cm^{-1}. J Mol Spectrosc 2007;246:133-57.

16. Toth RA, Miller CE, Brown LR, Devi VM, Benner DC. Line Positions and strengths of $^{16}O^{12}C^{18}O$, $^{18}O^{12}C^{18}O$ and $^{17}O^{12}C^{18}O$ between 2200 and 7000 cm^{-1}. J Mol Spectrosc 2007;243:43-61.

17. Toth RA, Brown LR, Miller CE, Devi VM, Benner DC. Spectroscopic database of CO_2 line parameters: 4300-7000 cm^{-1}. J Quant Spectrosc Radiat Transf 2008;109:906-21.

18. Devi VM, Benner DC, Brown LR, Miller CE, Toth RA. Line mixing and speed dependence in CO_2 at 6227.9 cm^{-1}: constrained multispectrum analysis of intensities and line shapes in the 30013-00001 band. J Mol Spectrosc 2007;245:52-80.

19. Devi VM, Benner DC, Brown LR, Miller CE, Toth RA. Line mixing and speed dependence in CO_2 at 6348 cm^{-1}. Positions and intensities, and air- and self-broadening derived with constrained multispectrum analysis. J Mol Spectrosc 2007;242:90-117.

20. Predoi-Cross A, Unni AV, Liu W, Schofield I, Holladay C, McKeller ARW, Hurtmans D. Line shape parameters measurement and computations for self-broadened carbon dioxide transitions in the 30012-00001 and 30013-00001 bands, line mixing and speed dependence. J Mol Spectrosc 2007;245:34-51.

21. Predoi-Cross A, Liu W, Holladay C, Unni AV, Schofield I, McKellar ARW, et al. Line profile study of transitions in the 30012-00001 and 30013-0001 bands of carbon dioxide perturbed by air. J Mol Spectrosc 2007;246:98-112.

22. Hartmann JM, Tran H, Toon GC. Influence of line mixing on the retrievals of atmospheric CO_2 from space in the 1.6 and 2.1 μm regions. Atmos Chem Phys 2008;9:7303-12. http://dx.doi.org/10.5194/acp-9-7303-2009.

23. Povey C, Predoi-Cross A. Computations of temperature dependences for line shape parameters in the 30012-00001 and 30013-00001 bands of pure CO_2. J Mol Spectrosc 2009;257:187-99.

24. Predoi-Cross A, McKellar ARW, Benner DC, Devi VM, Gamache RR, Miller CE, et al. Temperature dependences of air-broadened Lorentz half-width and pressure shift coefficients in the 30013←00001 and 30012←00001 bands of CO_2 near 1600 nm. Can J Phys 2009;87:517-35.

25. Predoi-Cross A, Liu W, Murphy R, Povey C, Gamache RR, Laraia AL, et al. Measurements and computations for temperature dependences of self-broadened carbon dioxide transitions in the 30012-00001 and 30013-00001 bands. J Quant Spectrosc Radiat Transf 2010;111:1065-79.

26. Hartmann JM, Tran H, Ngo NH, Landsheere X, Chelin P, Lu Y, et al. Ab initio calculations of the spectral shapes of CO_2 isolated lines including non-Voigt effects and comparisons with experiments. Phys Rev A. 2013;87:013403.

27. Long DA, Truong C.-W, Hodges JT, Miller CE. Absolute $^{12}C^{16}O_2$ transition frequencies at the kHz-level from 1.6 to 7.8 μm. J Quant Spectrosc Radiat Transf 2013;130:112-15.

28. Lamouroux J, Gamache RR, Laraia AL. Semiclassical calculations of half-widths and line shifts for transitions in the 30012-00001 and 30013-00001 bands of CO_2. III. Self collisions. J Quant Spectrosc Radiat Transf 2012;113:1536-46.

29. Miller CE, Brown LR. Near infrared spectroscopy of carbon dioxide. I. $^{16}O^{12}C^{16}O$ line positions. J Mol Spectrosc 2004;228:329-54.

30. Miller CE, Montgomery MA, Onorato RM, Johnstone C, McNicholas TP, Kovaric B, et al. Near infrared spectroscopy of carbon dioxide. II: $^{16}O^{13}C^{16}O$ and $^{16}O^{13}C^{18}O$ line positions. J Mol Spectrosc 2004;228:355-74.

31. Larcher G, Tran H, Schwell M, Chelin P, Landsheere X, Hartmann J-M, Hu S-M. CO_2 isolated line shapes by classical molecular dynamics simulations: Influence of the intermolecular potential and comparison with new measurements. J Chem Phys 2014;140:084308.

32. Larcher G, Landsheere X, Schwell M, Tran H. Spectral shape parameters of pure CO_2 transitions near1.6 μm by tunable diode laser spectroscopy. J Quant Spectrosc Radiat Transf 2015;164:82–88.

33. Benner DC, Rinsland CP, Devi VM, Smith MAH, Atkins D. A multispectrum nonlinear least-squares fitting technique. J Quant Spectrosc Radiat Transf 1995;53:705-21.

34. Letchworth KL, Benner DC. Rapid and accurate calculation of the Voigt functions. J Quant Spectrosc Radiat Transf 2007;107:173-92.

35. Levy A, Lacome N, Chackerian Jr. C. Collisional line mixing In: Rao K Narahari, Weber Alfons, editors. Spectroscopy of the earth's atmosphere and interstellar medium. San Diego, CA. Academic Press, Inc. 1992 (Chapter 4).

36. Vitcu A. Line shape studies in the 0310-0110 Q branch of N_2O using a mid-infrared difference frequency spectrometer. Dissertation, University of Toronto, 2003.

37. Mantz AW, Sung K, Crawford TJ, Brown LR, Smith MAH, Devi VM, et al. A cryogenic Herriott cell vacuum coupled to a FT-IR JPL Bruker IFS-125 HR. J Mol Spectrosc 2014;304:12-24.

38. Rothman LS, Jacquemart D, Barbe J, Benner DC, Birk M, Brown LR, et al. The HITRAN2004 molecular spectroscopic database. J Quant Spectrosc Radiat Transf 2005;96:139-204.

39. Rothman LS, Gordon IE, Barbe A, Benner DC, Bernath PF, Birk M, et al. The HITRAN2008 molecular spectroscopic database. J Quant Spectrosc Radiat Transf 2009;110:533-72.

40. Rothman LS, Gordon IE, Babikov Y, Barbe A, Benner DC, Bernath PF, et al. The HITRAN2012 molecular spectroscopic database. J Quant Spectrosc Radiat Transf 2013;130:4-50.

41. Pollock CR, Petersen PR, Jennings DA, Wells JS, Maki AG. Absolute frequency measurements of the 2-0 band of CO at 2.3 μm; calibration standard frequencies from high resolution color center laser spectroscopy. J Mol Spectrosc 1983;99:357-68.

42. Swann WC, Gilbert SL. Pressure induced shift and broadening of 1510-1540-nm acetylene wavelength calibration lines. J Opt Soc Am B 2000;17:1263-70.

43. Gamache RR [unpublished results, 2015].

44. Wattson RB, Rothman LS. Direct numerical diagonalization: wave of the future. J Quant Spectrosc Radiat Transf 1992;48:763-80.

45. Tashkun SA, Perevalov VI, Teffo J-L, Bykov AD, Lavrentieva. CDSD-1000, the high-temperature carbon dioxide spectroscopic databank. J Quant Spectrosc Radiat Transf 2003;82:165-96.

46. Tashkun SA, Perevalov VI, Gamache RR, Lamouroux J. CDSD-296, high resolution carbon dioxide spectroscopic databank: Versions for atmospheric applications. J Quant Spectrosc Radiat Transf 2015;152:45-73.

47. Polyansky OL, Bielska K, Ghysels M, Lodi L, Zobov NF, Hodges JT, Tennyson J. High-accuracy CO_2 line intensities determined from theory and experiment. Phys Rev Lett 2015;114:243001-5.

48. Huang X. [Private communication, Dec. 2015].

49. Zak E, Tennyson J, Polyansky OL, Lodi L, Zobov NF, Tashkun SA, Perevalov VI. A room temperature CO_2 linelist with accurate intensities. J Quant Spectrosc Radiat Transf (accepted) 2015.

50. Hodges JT. National Institute of Standards and Technology, Private communication (2015).

51. Majcherova Z, Macko P, Romanini D, Perevalov VI, Tashkun SA, Teffo J-L, Campargue A. High-sensitivity CW-cavity ringdown spectroscopy of $^{12}CO_2$ near 1.5 μm. J Mol Spectrosc 2005;230:1-21.

52. Lin H, Reed ZD, Sironneau VT, Hodges JT. Cavity ring-down spectrometer for high-fidelity molecular absorption measurements. J Quant Spectrosc Radiat Transf 2015;161:11-20.

53. Burkart J, Saia T, Romanini D, Marangoni M, Campargue A, Kassi S. Communication: Saturated CO_2 absorption near 1.6 μm for kilohertz-accuracy transition frequencies. J Chem Phys 2015;141:191103.

54. Gamache RR, Rothman LS. Extension of the HITRAN Database to Non-LTE Applications. J Quant Spectrosc Radiat Transf 1992;48:519-25.

55. Gamache RR, Goldman A. Einstein A coefficient, integrated band intensity, and population factors: Application to the a $^1\Delta_g - X^3\Sigma_g^-$ (0,0) O_2 band. J Quant Spectrosc Radiat Transf 2001;69:389-401.

56. Rinsland CP, Benner DC, Devi VM. Absolute line intensities in CO_2 bands near 4.8 μm. Appl Opt 1986;25:1204-14.

57. Gamache RR, Lamouroex J. Predicting accurate line shape parameters for CO_2 transitions. J Quant Spectrosc Radiat Transf 2013;130:158-71, doi: 10.10.1016/j.jqsrt.2013.05.021.

58. Lamouroux J, Tran H, Laraia AL, Gamache RR, Rothman LS, Gorgon IE, Hartman J-M. Updated database plus software for line-mixing in CO_2 infrared spectra and their test using laboratory spectra in the 1.5-2.3 μm region. J Quant Spectrosc Radiat Transf 2010;111:2321-2331.

59. Lisak D, Cygan A, Wcislo P, Ciurylo R. Quadratic speed dependence of collisional broadening and shifting for atmospheric applications. J Quant Spectrosc Radiat Transf 2015;151:43-8.

60. Tran H, Ngo NH, Hartmann JM. Efficient computation of some speed-dependent isolated line shapes. J Quant Spectrosc Radiat Transf 2013;129:199-203.

Figures

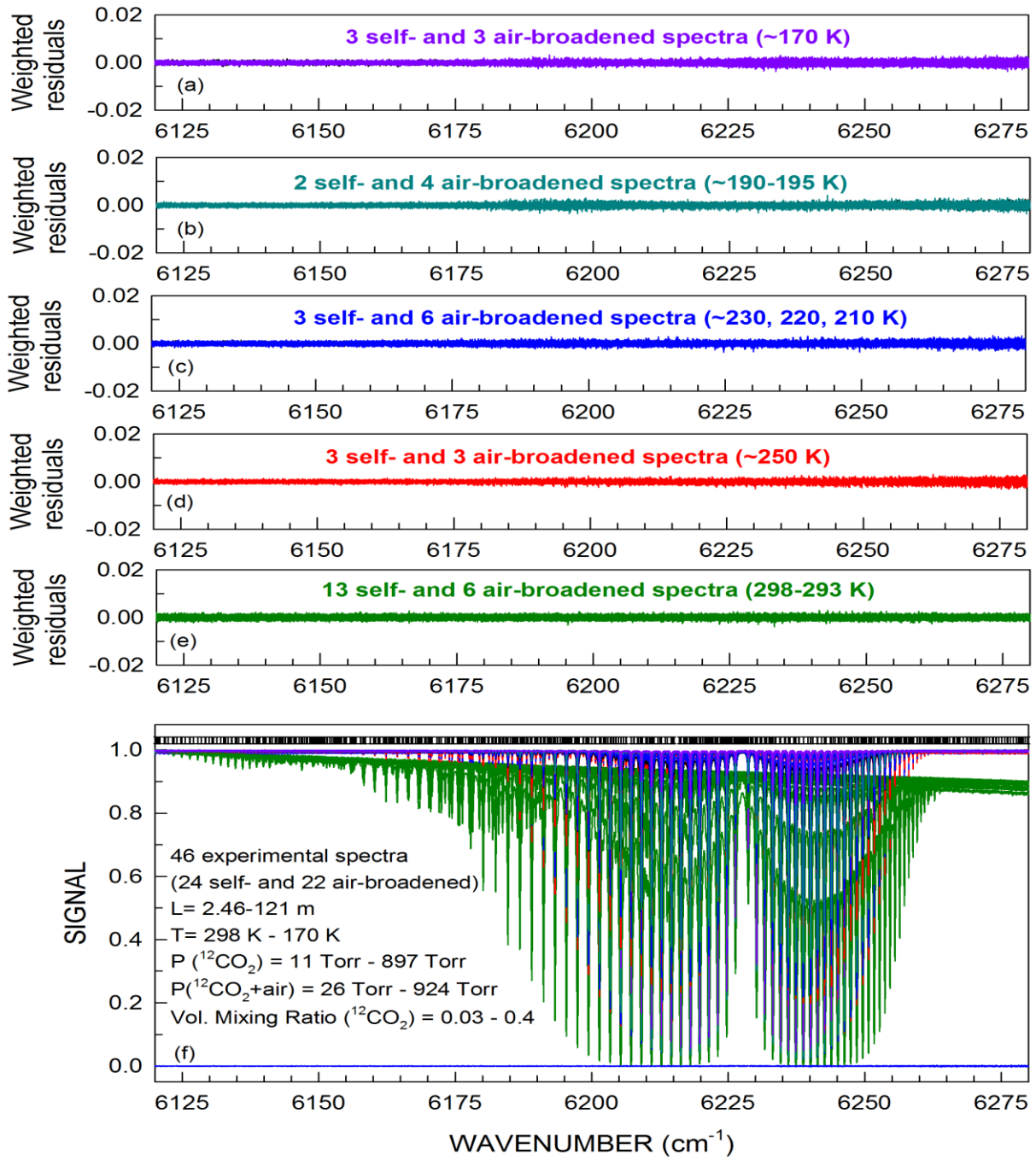

Fig. 1

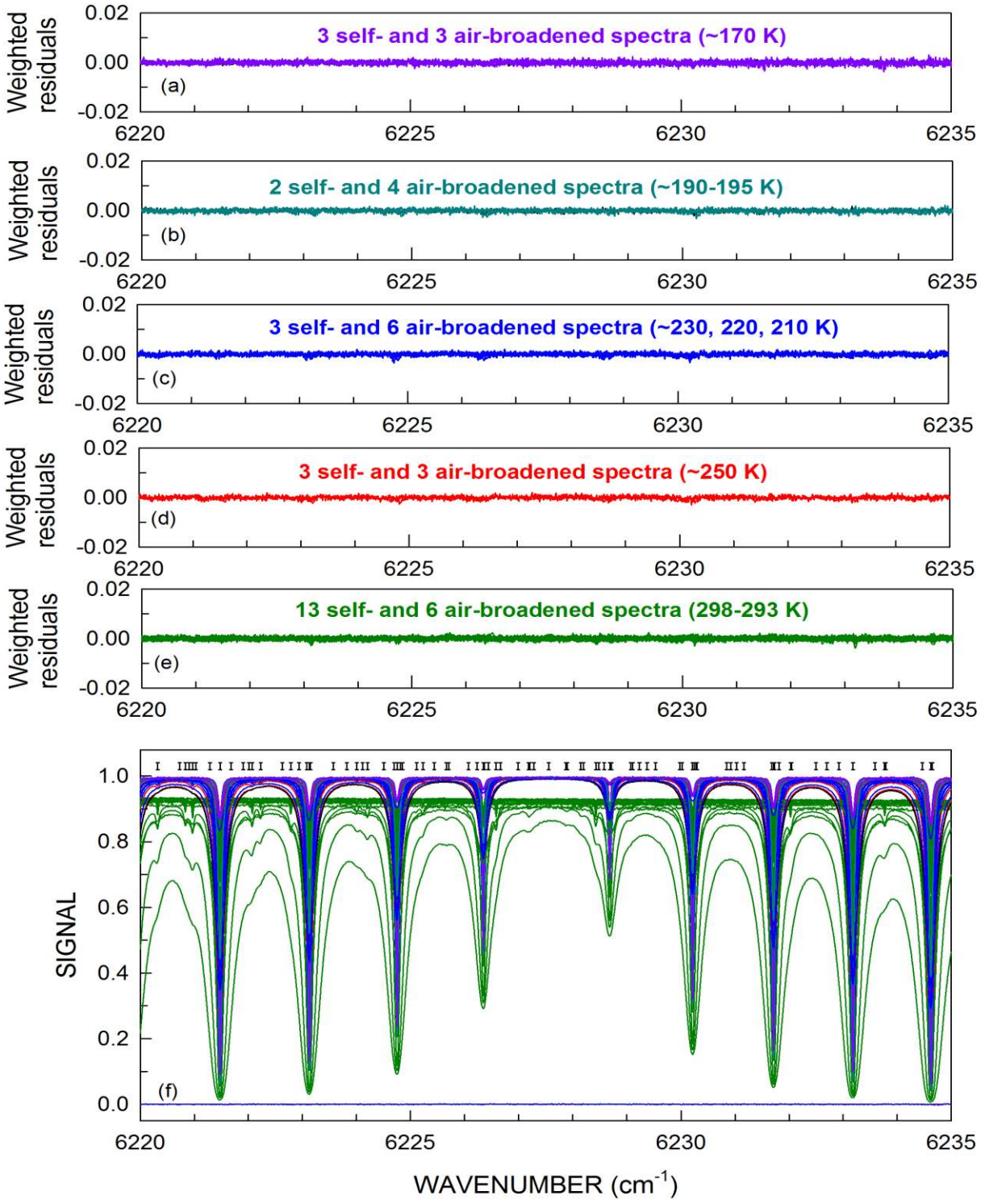
Weighted residuals
0.02
0.00
-0.02
3 self- and 3 air-broadened spectra (~170 K)
(a)
2 self- and 4 air-broadened spectra (~190-195 K)
(b)
3 self- and 6 air-broadened spectra (~230, 220, 210 K)
(c)
3 self- and 3 air-broadened spectra (~250 K)
(d)
13 self- and 6 air-broadened spectra (298-293 K)
(e)
6220
6225
6230
6235
SIGNAL
1.0
0.8
0.6
0.4
0.2
0.0
(f)
WAVENUMBER (cm-1)

Fig. 2

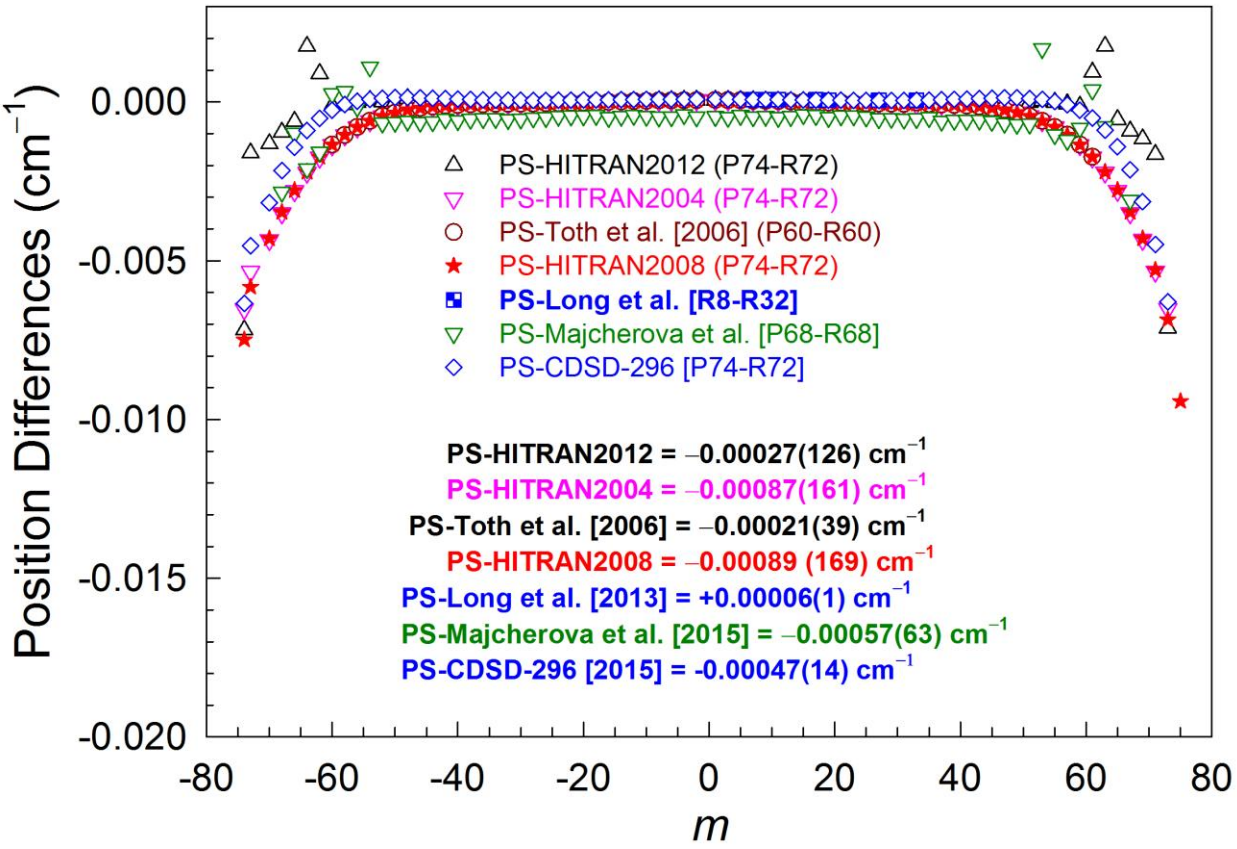
Position Differences (cm^{-1})
0.000
-0.005
-0.010
-0.015
-0.020
-80
-60
-40
-20
0
20
40
60
80
m
PS-HITRAN2012 (P74-R72)
PS-HITRAN2004 (P74-R72)
PS-Toth et al. [2006] (P60-R60)
PS-HITRAN2008 (P74-R72)
PS-Long et al. [R8-R32]
PS-Majcherova et al. [P68-R68]
PS-CDSD-296 [P74-R72]
PS-HITRAN2012 = –0.00027(126) cm^{-1}
PS-HITRAN2004 = –0.00087(161) cm^{-1}
PS-Toth et al. [2006] = –0.00021(39) cm^{-1}
PS-HITRAN2008 = –0.00089 (169) cm^{-1}
PS-Long et al. [2013] = +0.00006(1) cm^{-1}
PS-Majcherova et al. [2015] = –0.00057(63) cm^{-1}
PS-CDSD-296 [2015] = -0.00047(14) cm^{-1}

Fig. 3

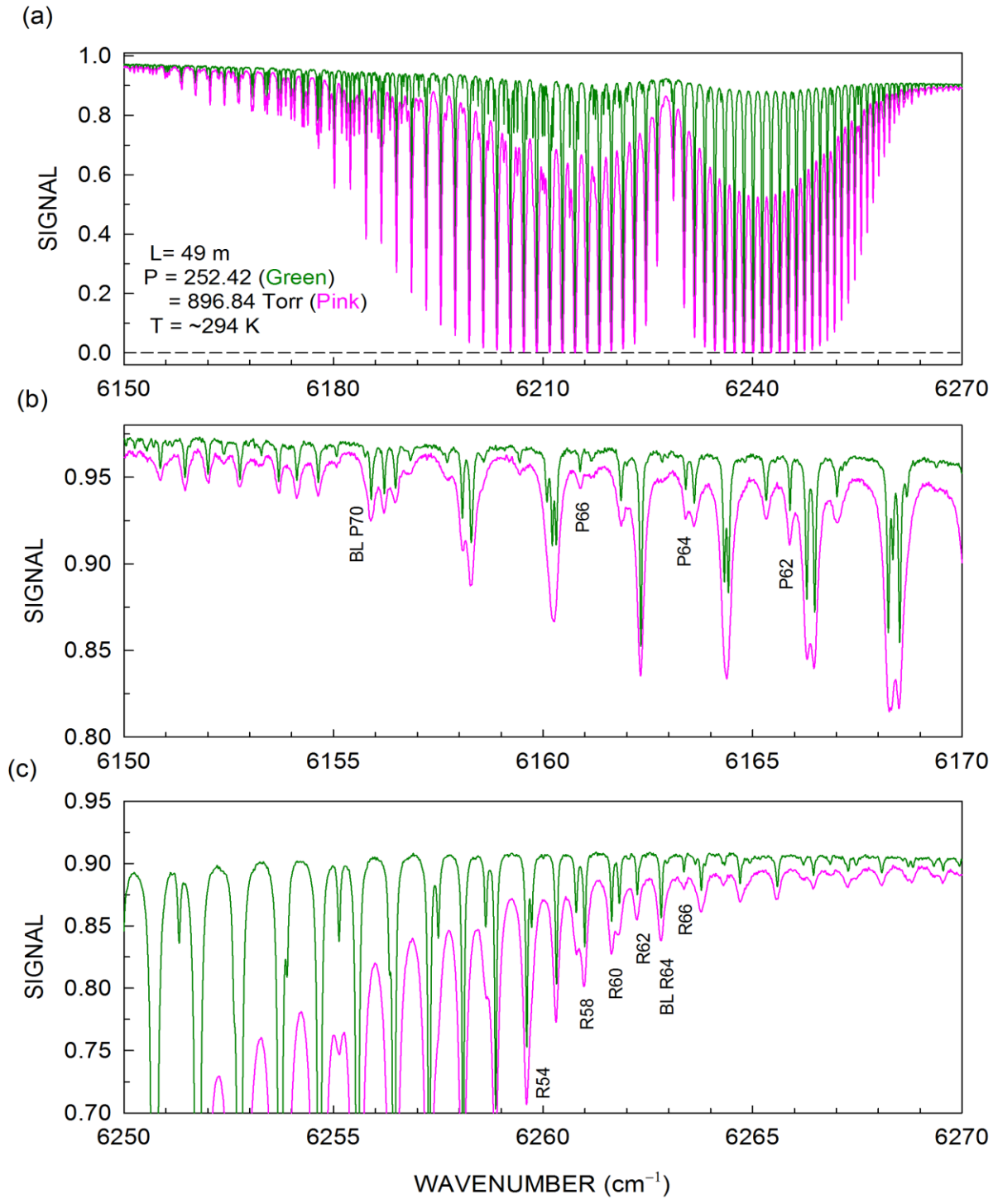
(a)
SIGNAL
L= 49 m
P = 252.42 (Green)
= 896.84 Torr (Pink)
T = ~294 K
(b)
SIGNAL
BL P70
P66
P64
P62
(c)
SIGNAL
R54
R58
R60
BL R64
R62
R66
WAVENUMBER (cm⁻¹)

Fig. 4

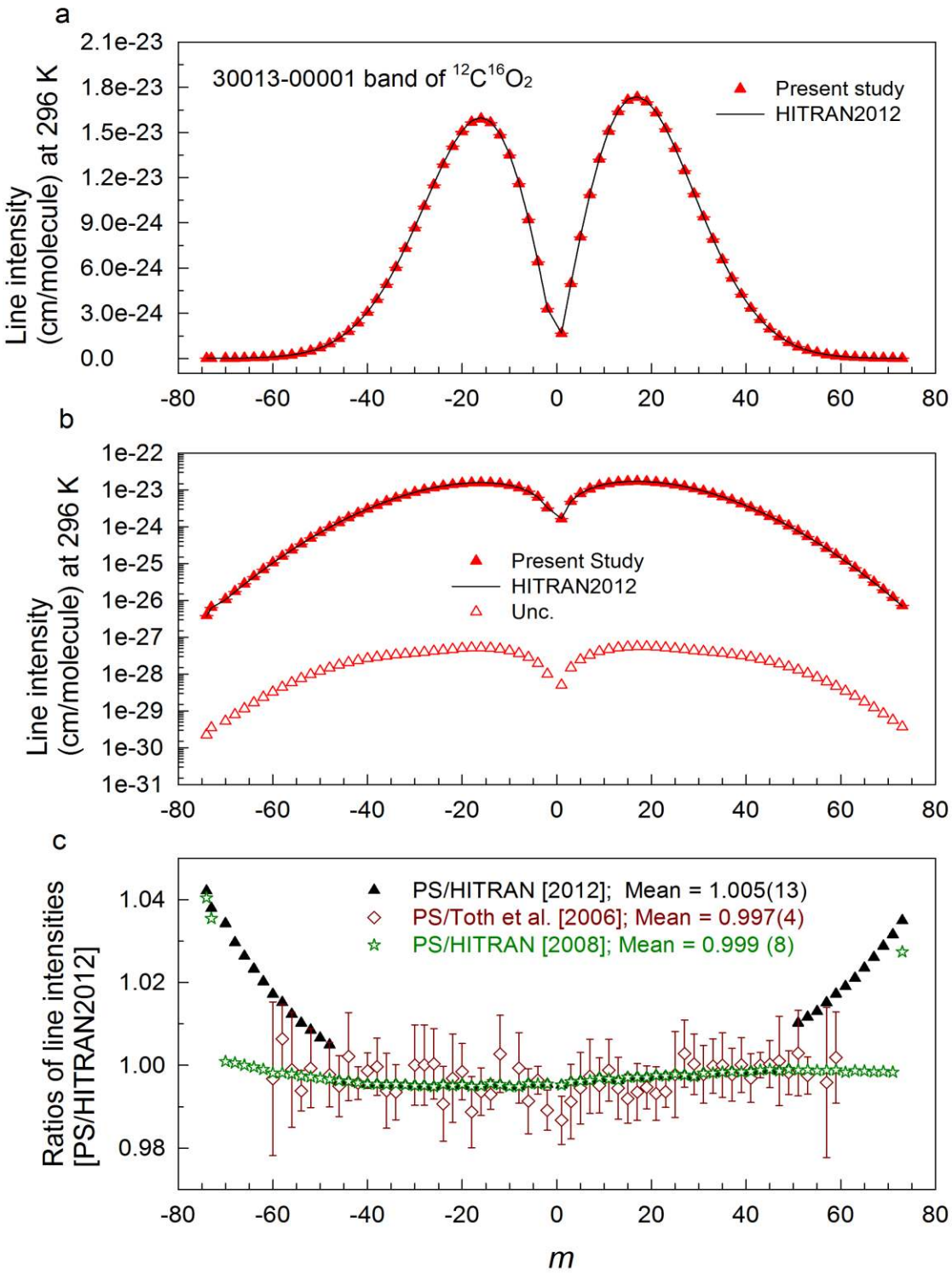
a
30013-00001 band of $^{12}C^{16}O_2$
Present study
HITRAN2012
Line intensity (cm/molecule) at 296 K
2.1e-23
1.8e-23
1.5e-23
1.2e-23
9.0e-24
6.0e-24
3.0e-24
0.0
b
Present Study
HITRAN2012
Unc.
Line intensity (cm/molecule) at 296 K
1e-22
1e-23
1e-24
1e-25
1e-26
1e-27
1e-28
1e-29
1e-30
1e-31
c
PS/HITRAN [2012]; Mean = 1.005(13)
PS/Toth et al. [2006]; Mean = 0.997(4)
PS/HITRAN [2008]; Mean = 0.999 (8)
Ratios of line intensities [PS/HITRAN2012]
1.04
1.02
1.00
0.98
-80
-60
-40
-20
0
20
40
60
80
m

Fig. 5

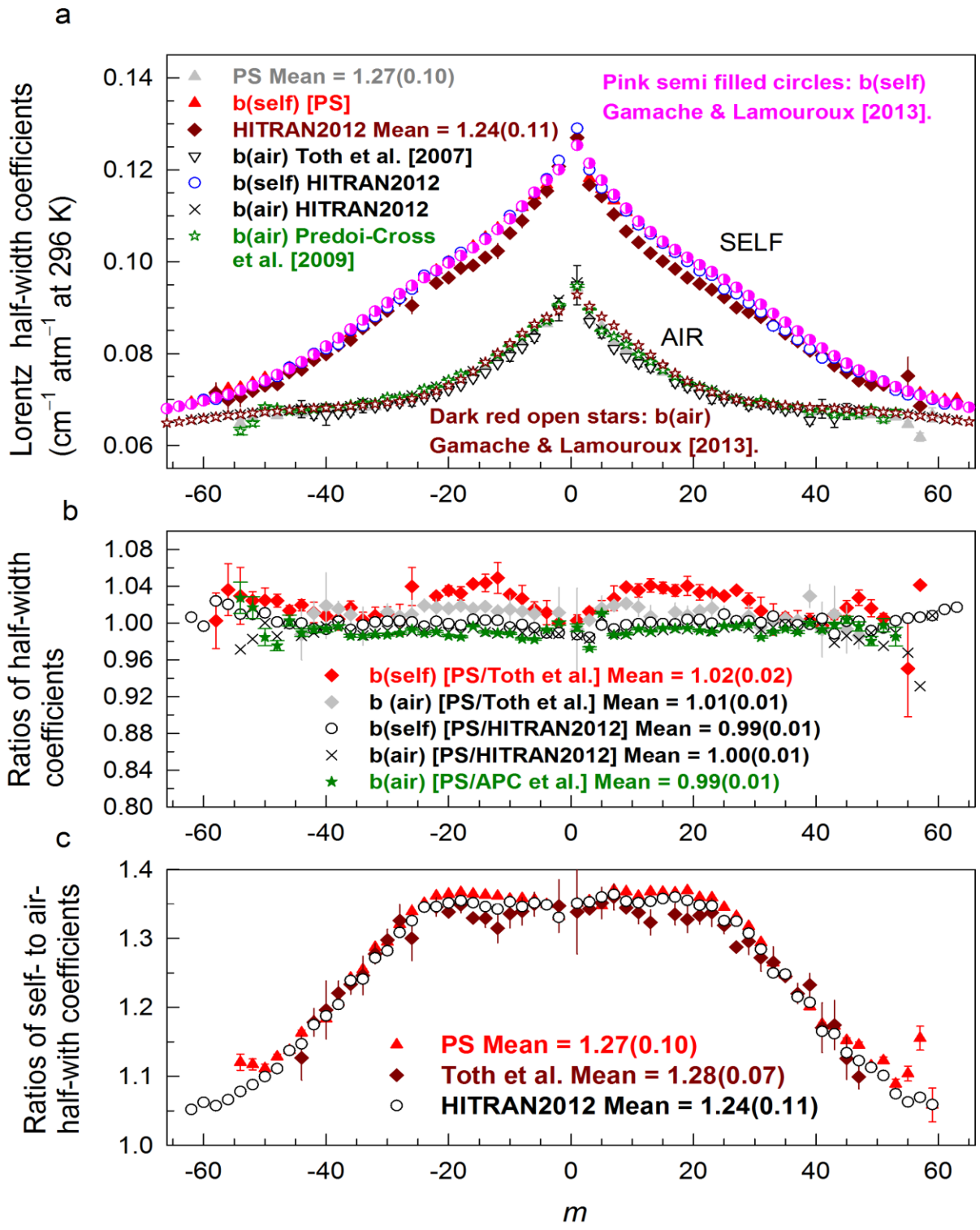
a
Lorentz half-width coefficients (cm^{-1} atm^{-1} at 296 K)
PS Mean = 1.27(0.10)
b(self) [PS]
HITRAN2012 Mean = 1.24(0.11)
b(air) Toth et al. [2007]
b(self) HITRAN2012
b(air) HITRAN2012
b(air) Predoi-Cross et al. [2009]
Pink semi filled circles: b(self) Gamache & Lamouroux [2013].
SELF
AIR
Dark red open stars: b(air) Gamache & Lamouroux [2013].
b
Ratios of half-width coefficients
b(self) [PS/Toth et al.] Mean = 1.02(0.02)
b (air) [PS/Toth et al.] Mean = 1.01(0.01)
b(self) [PS/HITRAN2012] Mean = 0.99(0.01)
b(air) [PS/HITRAN2012] Mean = 1.00(0.01)
b(air) [PS/APC et al.] Mean = 0.99(0.01)
c
Ratios of self- to air-half-with coefficients
PS Mean = 1.27(0.10)
Toth et al. Mean = 1.28(0.07)
HITRAN2012 Mean = 1.24(0.11)
m

Fig. 6

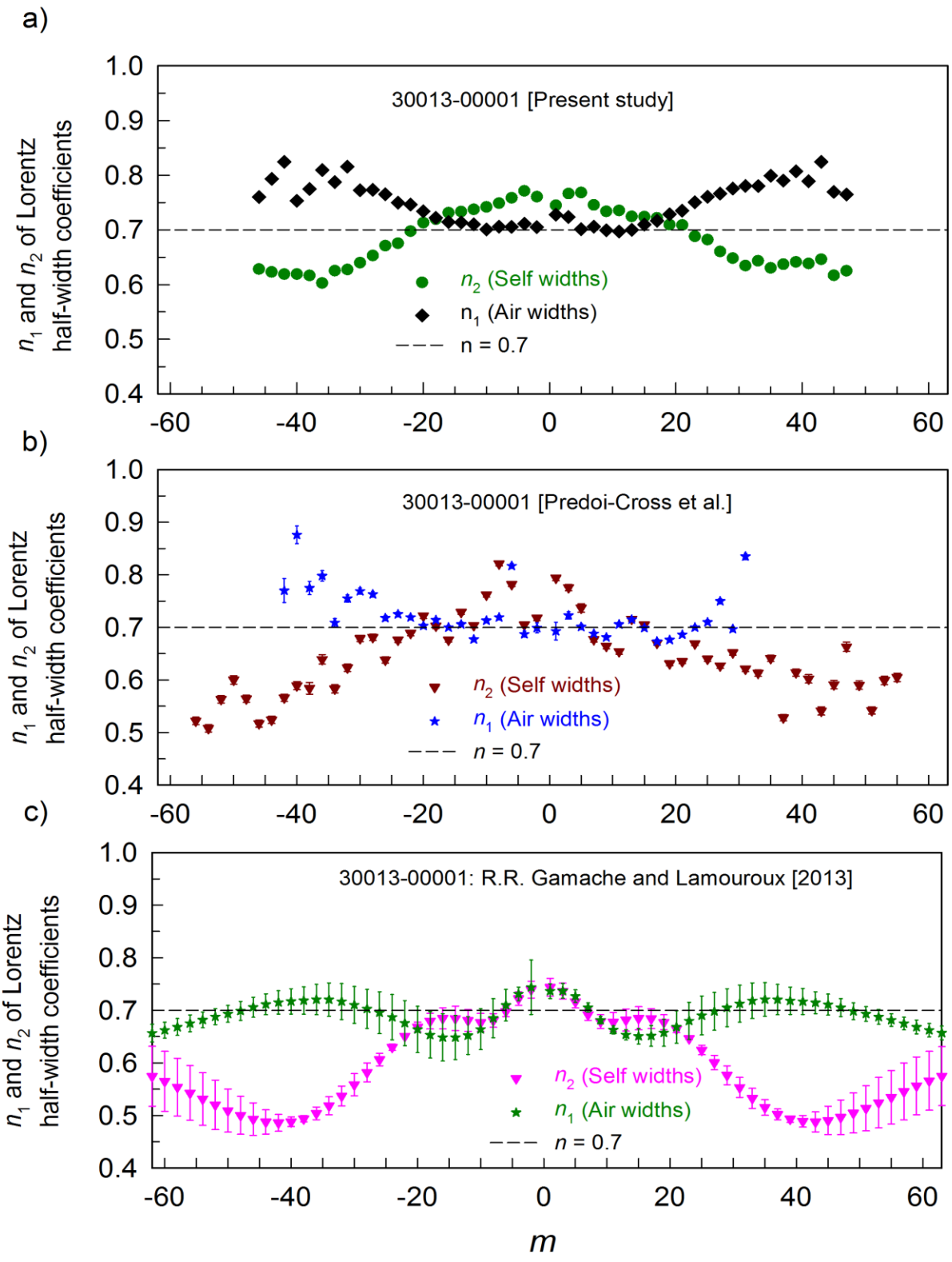
a)
30013-00001 [Present study]
n_2 (Self widths)
n_1 (Air widths)
n = 0.7
n_1 and n_2 of Lorentz half-width coefficients
b)
30013-00001 [Predoi-Cross et al.]
n_2 (Self widths)
n_1 (Air widths)
n = 0.7
n_1 and n_2 of Lorentz half-width coefficients
c)
30013-00001: R.R. Gamache and Lamouroux [2013]
n_2 (Self widths)
n_1 (Air widths)
n = 0.7
n_1 and n_2 of Lorentz half-width coefficients
1.0
0.9
0.8
0.7
0.6
0.5
0.4
-60
-40
-20
0
20
40
60
m

Fig. 7

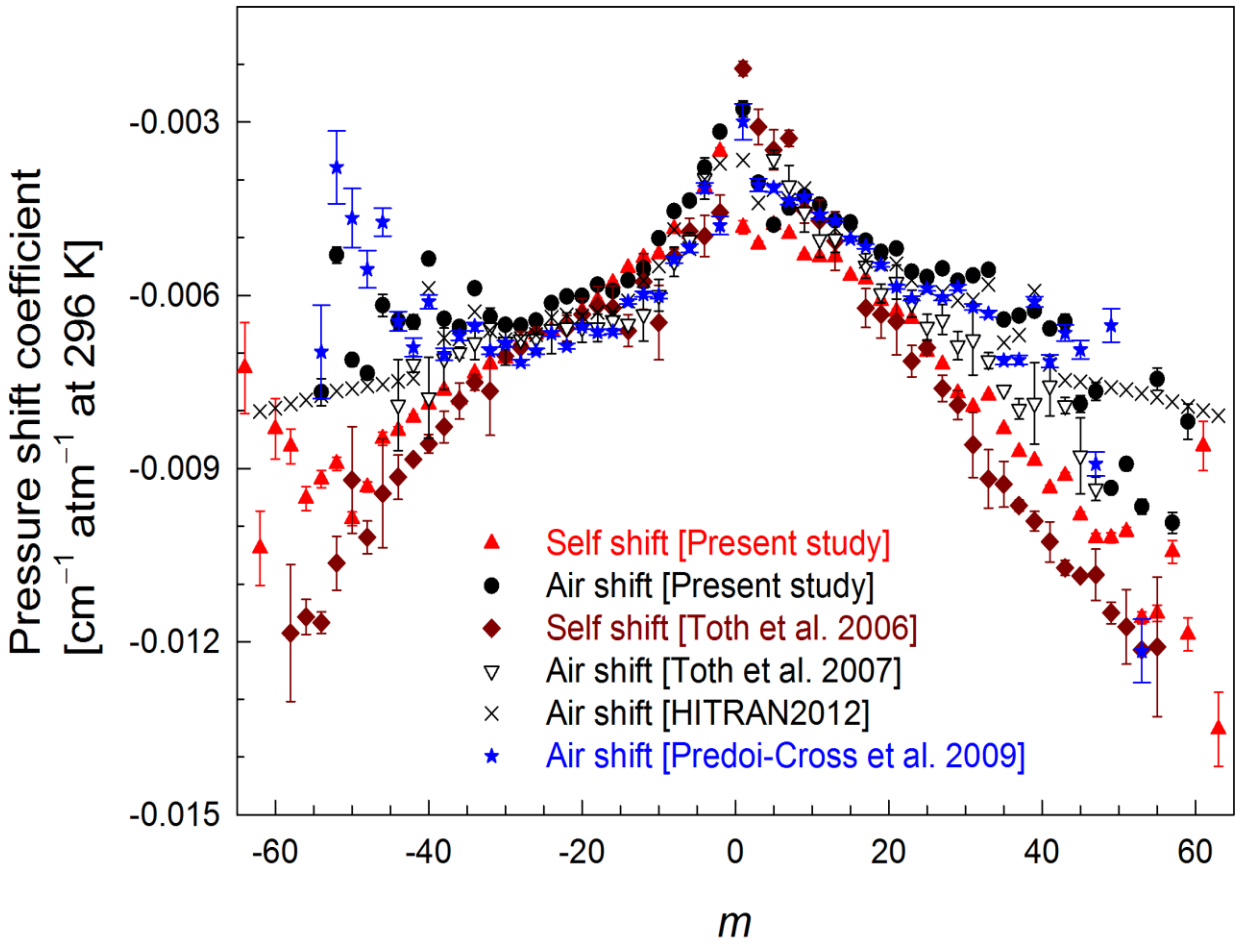
Pressure shift coefficient
[cm^{-1} atm^{-1} at 296 K]
-0.003
-0.006
-0.009
-0.012
-0.015
-60
-40
-20
0
20
40
60
m
Self shift [Present study]
Air shift [Present study]
Self shift [Toth et al. 2006]
Air shift [Toth et al. 2007]
Air shift [HITRAN2012]
Air shift [Predoi-Cross et al. 2009]

Fig. 8

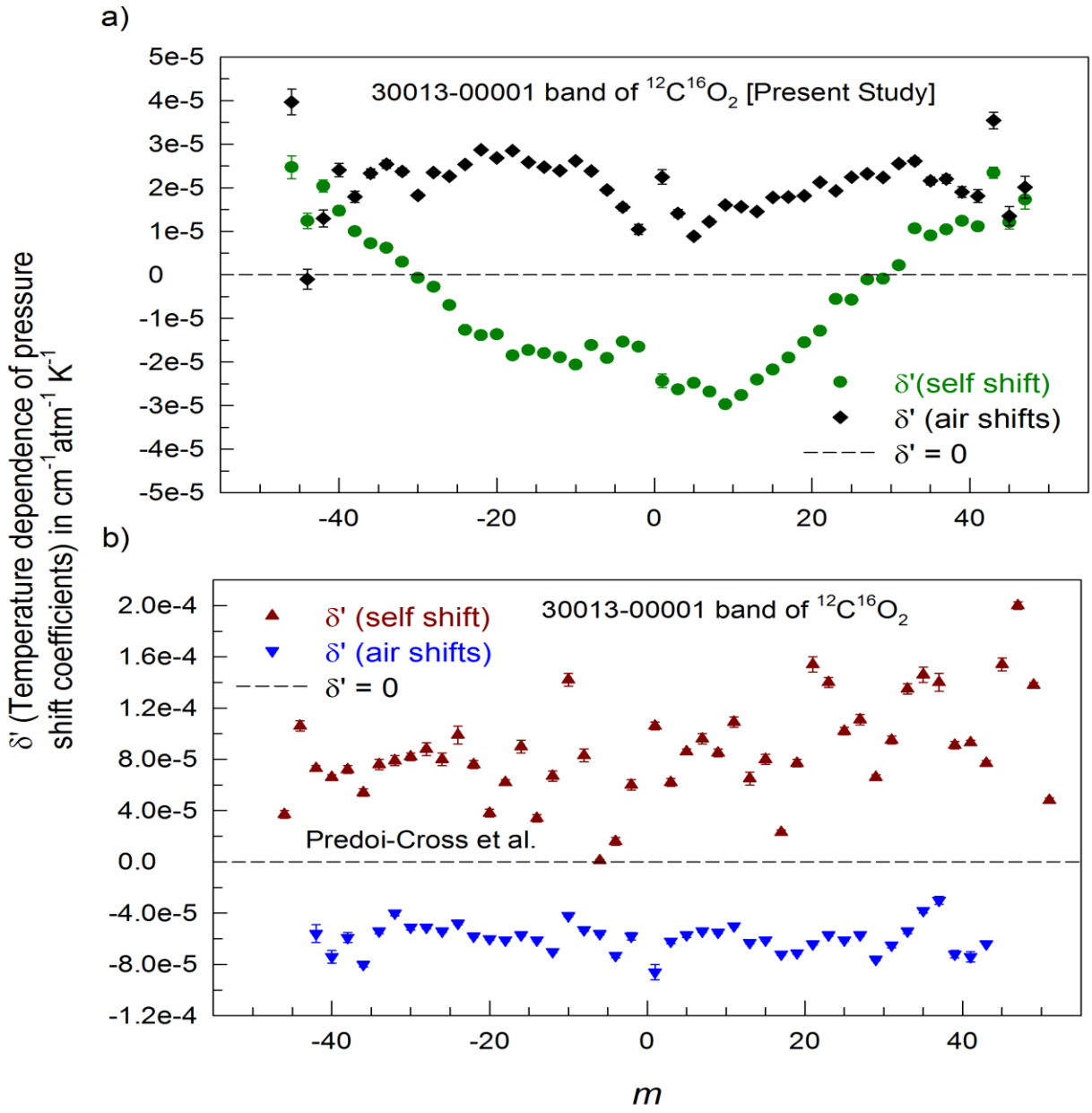
a)
30013-00001 band of $^{12}C^{16}O_2$ [Present Study]
δ'(self shift)
δ' (air shifts)
δ' = 0
b)
δ' (self shift)
δ' (air shifts)
δ' = 0
30013-00001 band of $^{12}C^{16}O_2$
Predoi-Cross et al.
δ' (Temperature dependence of pressure shift coefficients) in $cm^{-1}atm^{-1}K^{-1}$
m

Fig. 9

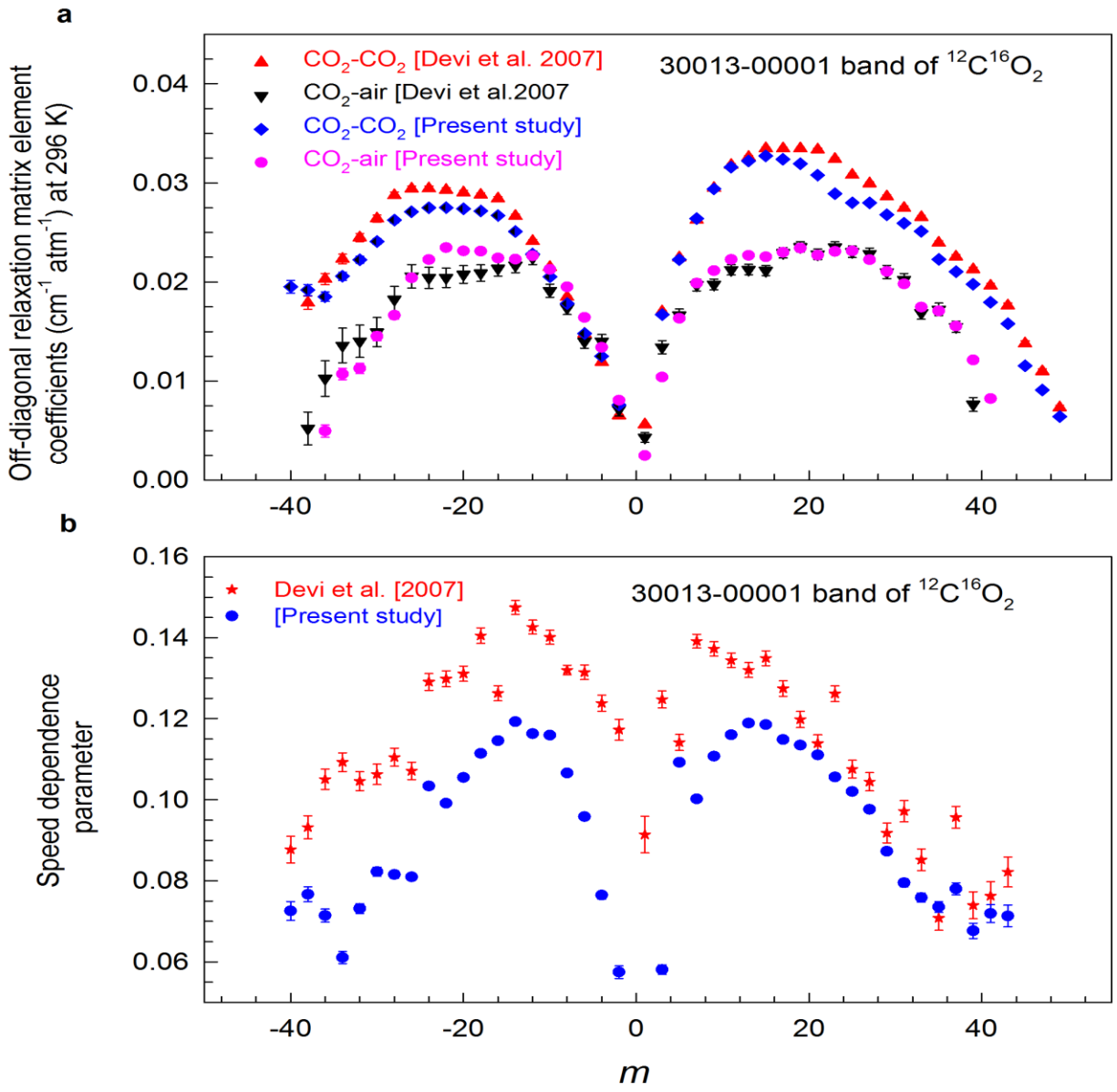
a
Off-diagonal relaxation matrix element coefficients (cm^{-1} atm^{-1}) at 296 K)
CO_2-CO_2 [Devi et al. 2007]
CO_2-air [Devi et al.2007
CO_2-CO_2 [Present study]
CO_2-air [Present study]
30013-00001 band of $^{12}C^{16}O_2$
0.04
0.03
0.02
0.01
0.00
-40
-20
0
20
40
b
Speed dependence parameter
Devi et al. [2007]
[Present study]
30013-00001 band of $^{12}C^{16}O_2$
0.16
0.14
0.12
0.10
0.08
0.06
-40
-20
0
20
40
m

Fig. 10

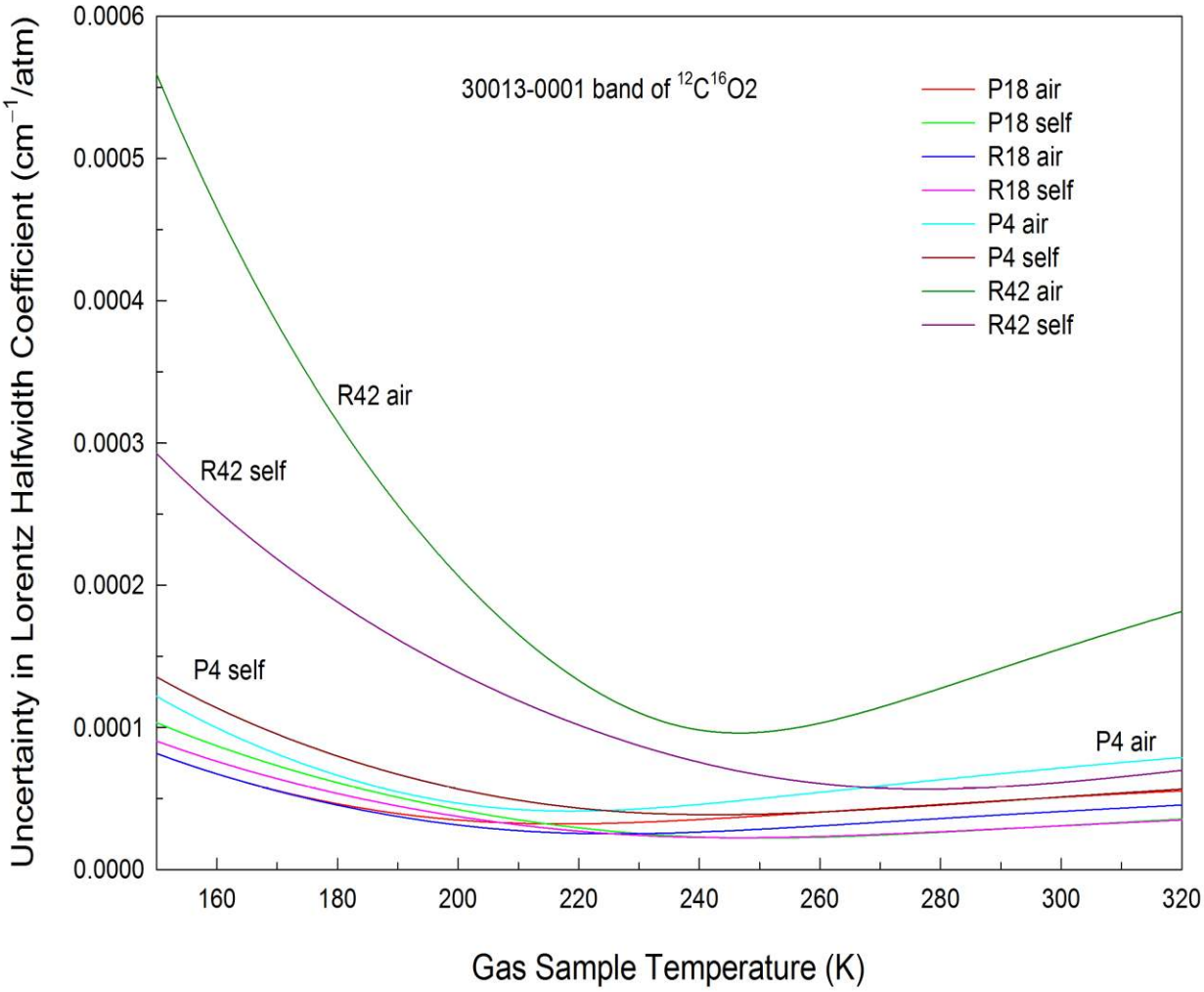
30013-0001 band of $^{12}C^{16}O2$
P18 air
P18 self
R18 air
R18 self
P4 air
P4 self
R42 air
R42 self
R42 air
R42 self
P4 self
P4 air
Uncertainty in Lorentz Halfwidth Coefficient (cm^{-1}/atm)
0.0006
0.0005
0.0004
0.0003
0.0002
0.0001
0.0000
160
180
200
220
240
260
280
300
320
Gas Sample Temperature (K)

Fig. 11

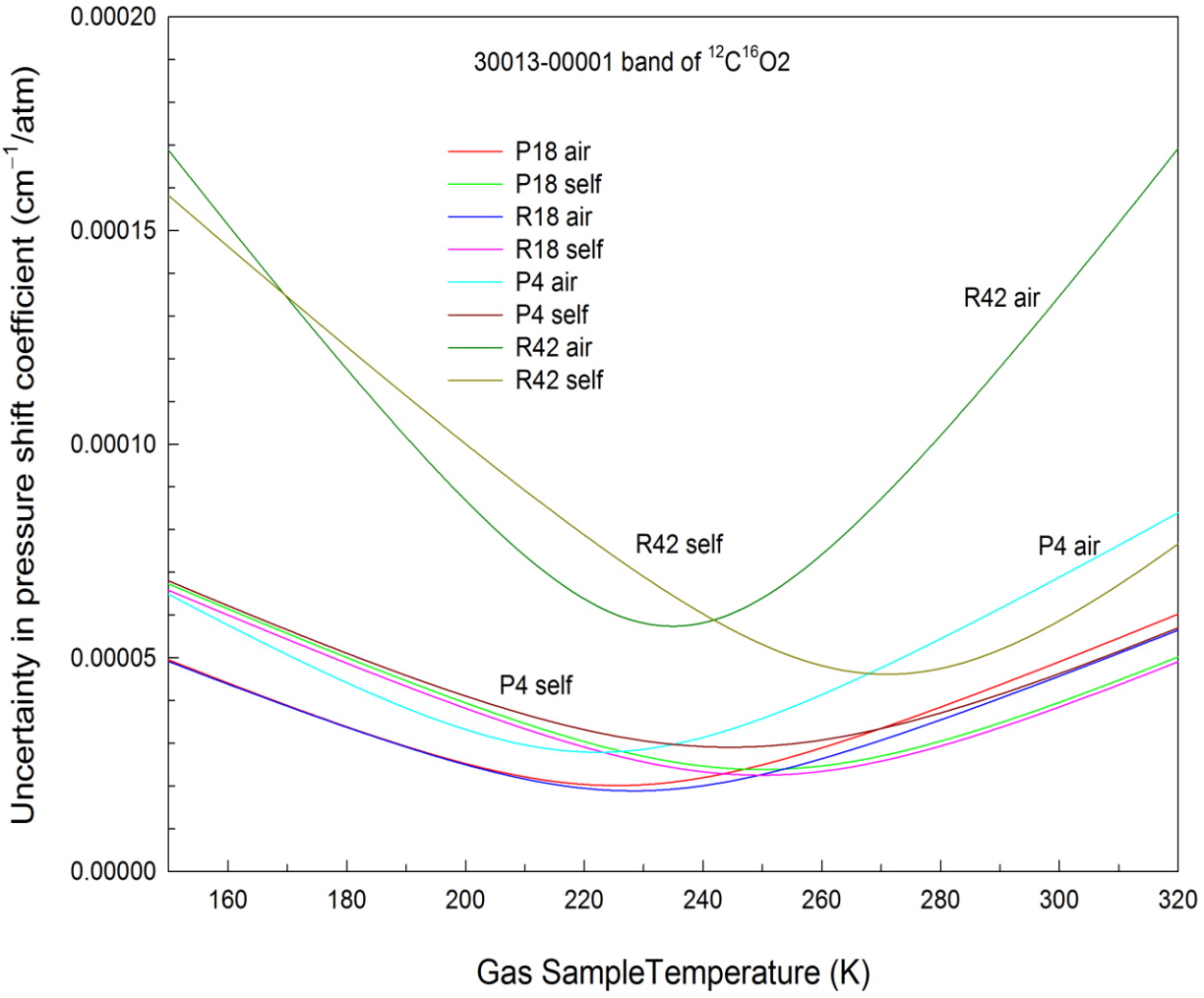
30013-00001 band of $^{12}C^{16}O2$
P18 air
P18 self
R18 air
R18 self
P4 air
P4 self
R42 air
R42 self
R42 air
R42 self
P4 air
P4 self
Uncertainty in pressure shift coefficient (cm^{-1}/atm)
0.00020
0.00015
0.00010
0.00005
0.00000
160
180
200
220
240
260
280
300
320
Gas SampleTemperature (K)

Fig. 12

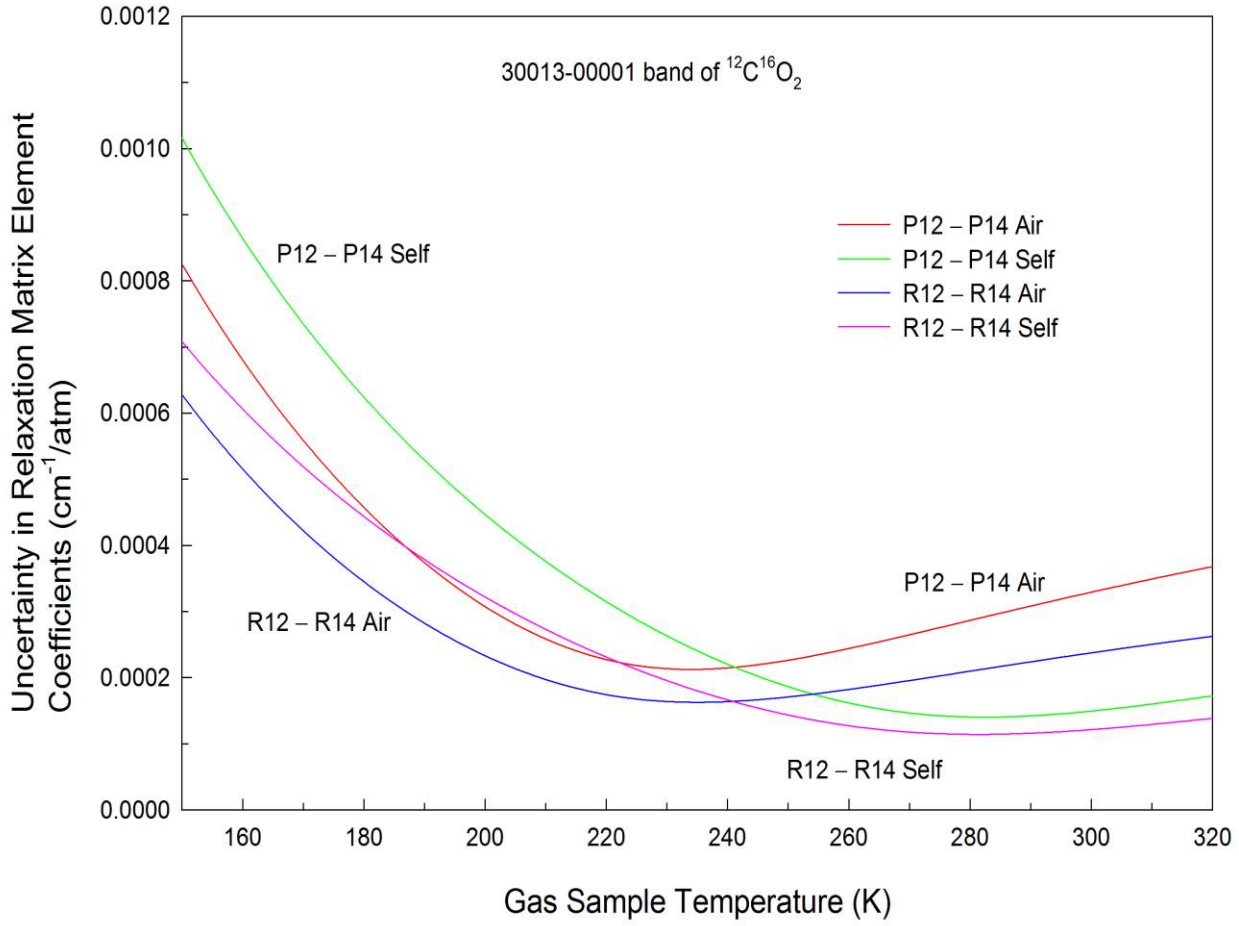
30013-00001 band of $^{12}C^{16}O_2$
Uncertainty in Relaxation Matrix Element
Coefficients (cm^{-1}/atm)
Gas Sample Temperature (K)
P12 – P14 Air
P12 – P14 Self
R12 – R14 Air
R12 – R14 Self
0.0012
0.0010
0.0008
0.0006
0.0004
0.0002
0.0000
160
180
200
220
240
260
280
300
320

Fig. 13

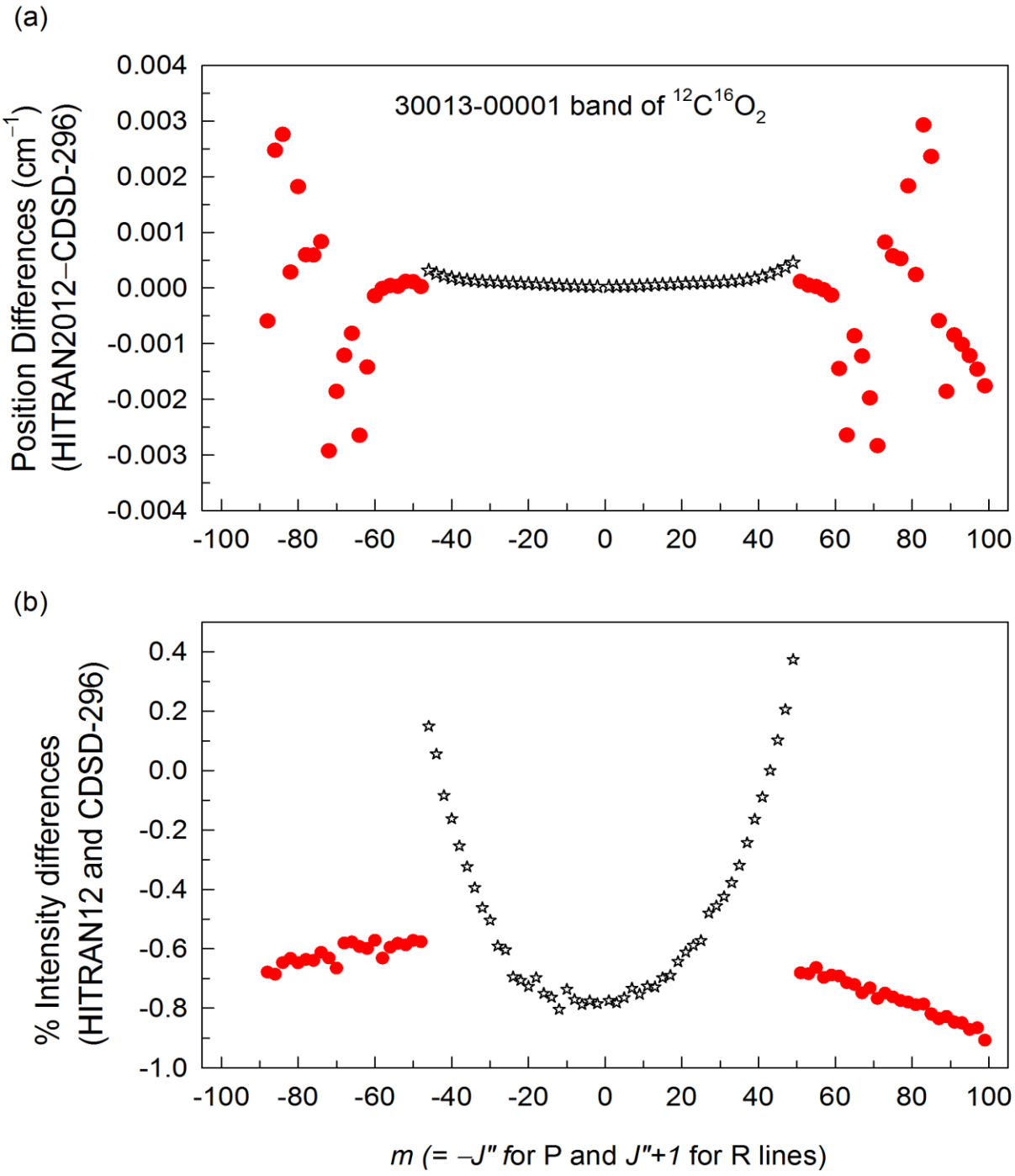
(a)
30013-00001 band of $^{12}C^{16}O_2$
Position Differences (cm^{-1})
(HITRAN2012–CDSD-296)
0.004
0.003
0.002
0.001
0.000
-0.001
-0.002
-0.003
-0.004
-100 -80 -60 -40 -20 0 20 40 60 80 100
(b)
% Intensity differences
(HITRAN12 and CDSD-296)
0.4
0.2
0.0
-0.2
-0.4
-0.6
-0.8
-1.0
-100 -80 -60 -40 -20 0 20 40 60 80 100
m (= –*J″* for P and *J″*+*1* for R lines)

Fig. 14

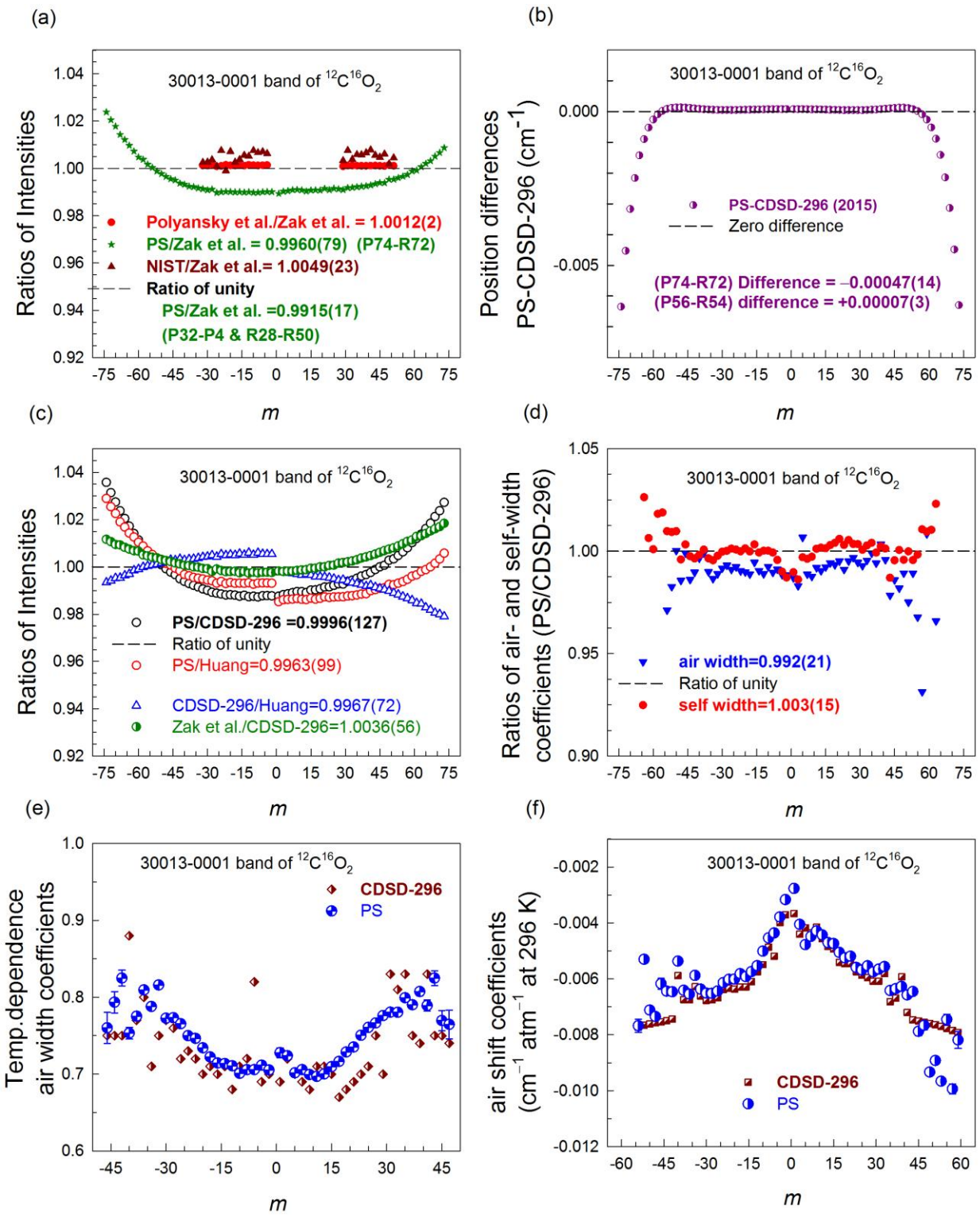
(a)
30013-0001 band of $^{12}C^{16}O_2$
Ratios of Intensities
Polyansky et al./Zak et al. = 1.0012(2)
PS/Zak et al. = 0.9960(79) (P74-R72)
NIST/Zak et al.= 1.0049(23)
Ratio of unity
PS/Zak et al. =0.9915(17)
(P32-P4 & R28-R50)
m
(b)
30013-0001 band of $^{12}C^{16}O_2$
Position differences PS-CDSD-296 (cm^{-1})
PS-CDSD-296 (2015)
Zero difference
(P74-R72) Difference = –0.00047(14)
(P56-R54) difference = +0.00007(3)
m
(c)
30013-0001 band of $^{12}C^{16}O_2$
Ratios of Intensities
PS/CDSD-296 =0.9996(127)
Ratio of unity
PS/Huang=0.9963(99)
CDSD-296/Huang=0.9967(72)
Zak et al./CDSD-296=1.0036(56)
m
(d)
30013-0001 band of $^{12}C^{16}O_2$
Ratios of air- and self-width coefficients (PS/CDSD-296)
air width=0.992(21)
Ratio of unity
self width=1.003(15)
m
(e)
30013-0001 band of $^{12}C^{16}O_2$
Temp.dependence air width coefficients
CDSD-296
PS
m
(f)
30013-0001 band of $^{12}C^{16}O_2$
air shift coefficients (cm^{-1} atm^{-1} at 296 K)
CDSD-296
PS
m

Fig. 15

Table 1

Summary of recent line shape measurements[a] (number and quantum number range) for the 30013←00001 band of $^{12}C^{16}O_2$.

Reference	Line shape	self-width[b]	n_2 (self width)[c]	self-shift[b]	δ' (self)[d]	air-width[b]	n_1 (air width)[c]	air-shift[b]	δ' (air)[d]
Present study	Speed dependent Voigt, Line mixing[e]	65 P66-R62	47 P46-R46	64 P64-R62	47 P46-R46	59 P54-R62	47 P46-R46	57 P54-P58	47 P46-R46
Devi et al. 2007 [**18**	Speed dependent Voigt, Line mixing[e]	63 P62-R62	None	63 P62-R6		53 P52-R52		53 P52-R52	
Toth et al. 2006 [**14**]	Voigt	57 P58-R56		54 P58-R54					
Toth et al. 2007 [**15**]	Voigt					44 P44-R46		46 P46-R46	
Predoi-Cross et al. (2007) [**20**]	Speed dependent Voigt, Line mixing	57 P56-R56		57 P56-R56					
Predoi-Cross et al. (2010) [**25**]	Voigt, line mixing, Speed-dependent-Voigt		56 P56-R54		49 P46-R50				
Predoi-Cross et al. (2007) [**21**]	Voigt, line mixing , Speed-dependent Voigt					57 P56-R56		57 P56-R57	
Predoi-Cross et al.[2009] [**24**]	Voigt, line mixing, Speed-dependent-Voigt					54 P54-R52	43 P42-R42	54 P54-R52	43 P42-R42

[a] All line shape studies published up to 2007 were discussed and compared in Predoi-Cross et al. [**21**]. However earlier results by Toth et al. [**14**,**15**] and Devi et al. [**18**], and measurements by Predoi-Cross et al. [**20**, **21**, **24**, **25**] are included in this Table. The reader may refer to the original articles for details.

[b] Lorentz half-width coefficients and pressure-shift coefficients are in $cm^{-1}atm^{-1}$ at 296 K.

[c] Temperature dependence exponents of air- and self-broadened half-width coefficients (n_1 and n_2) have no units.

[d] Temperature dependences of air- and self-shift coefficients, δ' (air) and δ' (self), are in cm^{-1} atm^{-1} K^{-1}.

[e] Line mixing using the off-diagonal relaxation matrix element coefficients. The temperature dependence exponents of the line mixing coefficients were also determined in the present study.

Table 2

Experimental setups and physical conditions of analyzed CO_2 spectra.

Parameters	**Kitt Peak FTS**	**JPL 125HR FTS:**
Light Source	Quartz halogen Lamp	Tungsten Lamp
Bean Splitter	CaF_2	CaF_2
Detector	Two matched InSb	InSb
Focal length of the collimating lens (mm)	2260	418
Source aperture diameter (mm)	8	1.3
Filter band pass (cm^{-1})	~3000–9000	~4200–6400
Resolution (cm^{-1}) Unapodized	~0.01	0.004–0.011
Max. Optical Path Difference (cm)	50	45–113
Pure Sample Pressure (Torr)	11–897	28-249
Total pressures of CO_2+air (Torr)	26–924	200-712
Volume mixing ratio	0.05–1.0	~0.03–1.0
Temperature (K)	~293–297	~170–250
Cell path length (m)	2.46, 24.94, 49.0, 121.18	20.941
Scanning time (h)	~1.5	~5–8
Signal-to-noise	800–1000	>2000
Gas Samples	$^{12}CO_2$[b, c]	^{12}C–enriched CO_2[c]
Calibration standards[a]	CO, C_2H_2	HCl

[a] Calibration of wavelength scales of spectra was achieved using CO/C_2H_2/HCl as appropriate (see the text for details).

[b] CO_2 sample with natural isotopic abundances.

[c] 99.99% ^{12}C-enhanced CO_2 sample.

Table 3

Summary of experimental conditions of the CO_2 spectra analyzed in this work.

Pure CO_2			**CO_2 in air**			
Temp (K)	Pressure (Torr)[a]	Path length (m)	Temp (K)	Pressure (Torr)[a]	CO_2 Volume mixing ratio	Path length (m)
293.99	896.84[b]	49.00	292.92	923.52[b]	0.0593	121.18
293.49	556.56[b]	49.00	293.07	250.38[b]	0.0595	121.18
293.49	252.42[b]	49.00	293.09	100.86[b]	0.0605	121.18
294.40	80.00[b]	49.00	293.05	549.545[b]	0.0499	49.00
293.09	52.14[b]	49.00	293.17	50.07[b]	0.0749	49.00
293.70	450.93[b]	24.94	292.63	26.05[b]	0.0679	49.00
293.70	101.95[b]	24.94	249.90	711.68	0.04436	20.941
293.94	26.10[b]	24.94	249.90	627.53	0.3960	20.941
294.05	11.04[b]	24.94	249.90	499.90	0.04436	20.941
294.37	94.65	2.46	230.10	709.48	0.2801	20.941
293.58	75.27[b]	2.46	230.10	350.26	0.2823	20.941
294.09	50.70	2.46	220.20	649.73	0.05085	20.941
293.57	25.61	2.46	220.20	502.02	0.05110	20.941
			210.20	499.94	0.3120	20.941
249.90	249.05	20.941	210.20	248.23	0.3132	20.941
249.90	101.90	20.941	195.00	496.96	0.03067	20.941
249.90	49.85	20.941	195.00	301.25	0.03066	20.941
230.00	199.45	20.941	190.30	422.85	0.2133	20.941
220.20	88.85	20.941	190.30	201.36	0.2146	20.941
210.30	155.15	20.941	170.30	181.73	0.2133	20.941
195.10	102.21	20.941	170.10	400.43	0.02985	20.941
195.00	47.74	20.941	170.10	200.41	0.02999	20.941
170.35	40.01	20.941	Spectra used only to check final results			
170.30	29.70	20.941	295.30	742.08	0.090341	32.54
170.00	33.78	20.941	293.20	550.67	0.090344	32.54

[a] 760 Torr = 1 atm = 101.3 kPa.

[b] Natural CO_2 sample (Volume Mixing Ratio = 1 with 0.9842 $^{16}O^{12}C^{16}O$). The rest of the spectra were obtained using a 99.99% ^{12}C-enriched CO_2 sample. Abundances of other isotopologues in the ^{12}C- enhanced sample were determined spectroscopically during the fitting in each spectrum.

Table 4

Measured line parameters and number of CO_2 measurements.

Parameters	Number of measurements	Parameters	Number of measurements
Position (ν)[a]	(585 total)[a] 522	Intensity (S)[b]	(585 total)[a] 522
Air-broadened width coefficient (air-width)[c]	110	Self-broadened width coefficient (self-width)[c]	178
Temperature dependence of air-broadened width coefficient[d] (n_1)	47	Temperature dependence of self-broadened width coefficient[d] (n_2)	47
Air- pressure-shift Coefficient (δ^0air)[c]	98	Self- pressure-shift coefficient (δ^0self)[c]	164
Temperature dependence of air-pressure-shift coefficient[e] (δ')	47	Temperature dependence of self- pressure-shift coefficient[e] (δ')	47
Off-diagonal relaxation matrix element coefficients for CO_2-air mixing (W_{ij})[c]	40	Off-diagonal relaxation matrix element coefficients for CO_2-CO_2 mixing (W_{ij})[c]	48
Temperature dependence of off-diagonal relaxation matrix element coefficients for CO_2-air mixing[c]	16	Temperature dependence of off-diagonal relaxation matrix element coefficients for CO_2-CO_2 mixing[c]	16
Speed dependence[d]	46	Auxiliary[f]	45

[a] Total numbers of measured positions and intensities. The positions and intensities determined using constraints are given in parentheses at the top of the row. The numbers given outside the parentheses correspond to those within the fitted region. The few lines outside of the fitted region correspond to constrained positions and intensities computed using the constants determined for the 30013←00001 band of $^{13}C^{16}O_2$ (below 6120 cm^{-1}) and the 40013←10001 band of $^{12}C^{16}O_2$ (beyond 6280 cm^{-1}). (See the Supplemental file for further details). Positions are in cm^{-1}.

[b] Line intensity in $cm^{-1}/(molecule\ cm^{-2})$ at 296 K.

[c] Lorentz half-width and pressure-shift coefficients and the off-diagonal relaxation matrix element coefficients in $cm^{-1}\ atm^{-1}$ at 296 K.

[d] Temperature dependence exponents of half-width coefficients, the off-diagonal relaxation matrix element coefficients and speed dependence have no units.

[e] Temperature dependences of pressure-shift coefficients are in units of cm^{-1} atm^{-1} K^{-1}.
[f] Examples of auxiliary parameters used in this study include position differences and intensity ratios (see the text for details).

Table 5

A sample of measured line parameters for the P40-R40 transitions in the 30013←00001 band of $^{12}C^{16}O_2$.

Line	Line position (unc.) [a]	Inten [b] x 10^{-24}	% Inten (unc)	half-width coeffs [c]	% unc.	n_1 or n_2 [d]	% unc.	Pressure shift δ^0 (unc.) [c]	T-dep. shift δ' (unc.) [e]	Speed depend. [f]	% unc.
P40	6191.171809(3)	3.072	0.009	0.06797 0.08045	0.19 0.07	0.7532 0.6192	1.01 0.53	-0.005366(11) -0.007887(50)	+0.241(15) +0.147(11)	0.0726	3.2
P38	6193.284448(2)	3.920	0.007	0.06804 0.08216	0.15 0.06	0.7751 0.6166	0.75 0.44	-0.006409(93) -0.007643(42)	+0.180(13) +0.100(9)	0.0767	2.4
P36	6195.367172(2)	4.915	0.006	0.06791 0.08440	0.12 0.06	0.8094 0.6028	0.57 0.38	-0.006548(74) -0.007803(39)	+0.233(10) +0.072(8)	0.0714	2.3
P34	6197.420175(2)	6.053	0.006	0.06837 0.08581	0.10 0.05	0.7877 0.6254	0.47 0.32	-0.005879(69) -0.007345(35)	+0.254(10) +0.062(7)	0.0611	2.4
P32	6199.443645(2)	7.319	0.005	0.06844 0.08810	0.09 0.05	0.8157 0.6274	0.37 0.29	-0.006370(59) -0.007187(35)	+0.238(8) +0.030(6)	0.0732	1.6
P30	6201.437761(2)	8.685	0.004	0.06962 0.09017	0.09 0.04	0.7725 0.6399	0.35 0.27	-0.006511(57) -0.007087(36)	+0.183(7) -0.007(6)	0.0823	1.4
P28	6203.402694(2)	10.11	0.004	0.06982 0.09221	0.07 0.03	0.7732 0.6531	0.30 0.23	-0.006522(48) -0.006789(34)	+0.235(6) -0.027(6)	0.0816	1.1
P26	6205.338606(2)	11.53	0.004	0.07027 0.09411	0.07 0.03	0.7653 0.6710	0.26 0.21	-0.006437(45) -0.006672(33)	+0.227(6) -0.069(5)	0.0810	1.0
P24	6207.245645(1)	12.89	0.003	0.07155 0.09667	0.08 0.04	0.7499 0.6754	0.28 0.21	-0.006136(49) -0.006599(36)	+0.254(6) -0.126(6)	0.1034	0.8
P22	6209.123953(1)	14.09	0.003	0.07210 0.09819	0.06 0.03	0.7464 0.6975	0.24 0.19	-0.006020(48) -0.006490(35)	+0.287(6) -0.138(6)	0.0992	0.7
P20	6210.973657(1)	15.06	0.003	0.07325 0.09993	0.05 0.03	0.7340 0.7130	0.23 0.17	-0.006011(46) -0.006268(35)	+0.268(6) -0.136(6)	0.1055	0.6
P18	6212.794874(1)	15.69	0.003	0.07446 0.10178	0.07 0.03	0.7221 0.7194	0.24 0.17	-0.005816(47) -0.006083(38)	+0.285(6) -0.185(6)	0.1114	0.6
P16	6214.587707(1)	15.91	0.003	0.07579 0.10343	0.05 0.03	0.7143 0.7312	0.22 0.15	-0.005922(45) -0.005782(35)	+0.259(6) -0.173(6)	0.1146	0.5
P14	6216.352248(1)	15.65	0.003	0.07726 0.10532	0.05 0.03	0.7135 0.7334	0.22 0.15	-0.005740(46) -0.005521(38)	+0.247(6) -0.180(6)	0.1193	0.5

P12	6218.088573(1)	14.85	0.003	0.07882 0.10732	0.05 0.03	0.7106 0.7374	0.23 0.15	-0.005530(46) -0.005346(36)	+0.239(6) -0.189(6)	0.1163	0.5
P10	6219.796748(2)	13.50	0.003	0.08069 0.10952	0.06 0.04	0.7009 0.7419	0.23 0.15	-0.005012(49) -0.005285(37)	+0.262(6) -0.206(6)	0.1159	0.5
P8	6221.476922(2)	11.61	0.003	0.08234 0.11182	0.06 0.04	0.7057 0.7488	0.24 0.16	-0.004542(53) -0.004848(37)	+0.239(7) -0.161(6)	0.1066	0.6
P6	6223.128831(2)	9.223	0.003	0.08435 0.11440	0.06 0.04	0.7057 0.7585	0.26 0.17	-0.004361(60) -0.004924(40)	+0.195(8) -0.191(7)	0.0958	0.7
P4	6224.752797(2)	6.415	0.003	0.08650 0.11672	0.08 0.04	0.7114 0.7712	0.31 0.18	-0.003787(66) -0.004121(44)	+0.156(8) -0.153(7)	0.0765	1.2
P2	6226.348728(2)	3.297	0.003	0.09063 0.12072	0.12 0.05	0.7052 0.7605	0.50 0.24	-0.003166(94) -0.003504(65)	+0.104(12) -0.165(9)	0.0575	2.7
R0	6228.690037(2)	1.670	0.003	0.09426 0.12737	0.21 0.07	0.7277 0.7448	0.88 0.34	-0.002768(14) -0.004821(11)	+0.225(17) -0.243(15)	0.0500	---
R2	6230.215814(2)	4.965	0.003	0.08720 0.11814	0.09 0.03	0.7237 0.7664	0.36 0.13	-0.004050(76) -0.005110(48)	+0.141(9) -0.263(7)	0.0581	2.0
R4	6231.713466(2)	8.076	0.003	0.08588 0.11575	0.07 0.04	0.7016 0.7683	0.29 0.18	-0.004780(55) -0.004777(40)	+0.089(7) -0.248(6)	0.1092	0.6
R6	6233.182934(2)	10.87	0.003	0.08266 0.11327	0.06 0.04	0.7057 0.7455	0.24 0.16	-0.004483(56) -0.004933(38)	+0.122(7) -0.268(7)	0.1002	0.6
R8	6234.624145(2)	13.24	0.003	0.08099 0.11079	0.06 0.04	0.6993 0.7337	0.23 0.15	-0.004284(50) -0.005307(38)	+0.161(6) -0.297(6)	0.1108	0.5
R10	6236.037013(1)	15.10	0.003	0.07926 0.10792	0.05 0.03	0.6969 0.7355	0.23 0.15	-0.004431(47) -0.005337(37)	+0.156(6) -0.276(6)	0.1160	0.5
R12	6237.421435(1)	16.40	0.003	0.07755 0.10608	0.05 0.03	0.7001 0.7246	0.23 0.15	-0.004703(45) -0.005330(37)	+0.145(6) -0.240(6)	0.1189	0.5
R14	6238.777296(1)	17.15	0.003	0.07601 0.10394	0.05 0.03	0.7096 0.7242	0.23 0.15	-0.004739(44) -0.005658(37)	+0.178(6) -0.217(6)	0.1185	0.5
R16	6240.104467(1)	17.34	0.003	0.07457 0.10190	0.05 0.03	0.7164 0.7219	0.22 0.15	-0.005054(43) -0.005721(37)	+0.179(6) -0.190(6)	0.1148	0.5
R18	6241.402807(1)	17.04	0.003	0.07331 0.10040	0.05 0.03	0.7286 0.7096	0.22 0.16	-0.005248(44) -0.006090(37)	+0.182(6) -0.155(6)	0.1135	0.5
R20	6242.672160(1)	16.32	0.003	0.07235 0.09838	0.06 0.03	0.7351 0.7089	0.23 0.17	-0.005189(44) -0.006277(36)	+0.213(6) -0.128(6)	0.1110	0.5
R22	6243.912358(1)	15.25	0.003	0.07136 0.09699	0.06 0.03	0.7504 0.6881	0.23 0.19	-0.005590(45) -0.006405(36)	+0.193(6) -0.055(6)	0.1056	0.6

R24	6245.123224(2)	13.94	0.004	0.07056 0.09491	0.06 0.03	0.7605 0.6821	0.24 0.19	-0.005683(41) -0.006979(35)	+0.225(5) -0.057(5)	0.1020	0.7
R26	6246.304565(2)	12.47	0.004	0.06998 0.09322	0.07 0.03	0.7663 0.6604	0.26 0.21	-0.005536(43) -0.007197(35)	+0.232(6) -0.011(5)	0.0976	0.8
R28	6247.456179(2)	10.93	0.004	0.06922 0.09121	0.07 0.03	0.7759 0.6482	0.28 0.23	-0.005749(46) -0.007694(35)	+0.224(6) -0.009(6)	0.0873	1.0
R30	6248.577855(2)	9.398	0.004	0.06881 0.08906	0.07 0.04	0.7804 0.6345	0.32 0.27	-0.005655(51) -0.007930(36)	+0.256(7) -0.022(6)	0.0795	1.2
R32	6249.669372(2)	7.925	0.005	0.06849 0.08664	0.09 0.04	0.7803 0.6433	0.37 0.28	-0.005560(58) -0.007930(36)	+0.262(8) +0.107(6)	0.0759	1.5
R34	6250.730499(2)	6.561	0.006	0.06804 0.08484	0.10 0.05	0.7992 0.6304	0.44 0.33	-0.006420(64) -0.008312(38)	+0.216(9) +0.090(7)	0.0736	1.8
R36	6251.760996(2)	5.334	0.006	0.06790 0.08284	0.12 0.05	0.7900 0.6370	0.56 0.38	-0.006353(74) -0.008711(40)	+0.220(10) +0.105(7)	0.0780	1.9
R38	6252.760618(3)	4.259	0.007	0.06733 0.08089	0.15 0.06	0.8073 0.6412	0.68 0.44	-0.006267(89) -0.008863(44)	+0.191(13) +0.124(8)	0.0677	2.8
R40	6253.729113(3)	3.342	0.009	0.06752 0.07940	0.18 0.08	0.7890 0.6386	0.91 0.50	-0.006577(10) -0.009339(49)	+0.181(15) +0.111(10)	0.0719	3.1

The uncertainties listed under the various columns correspond to one sigma internal statistical errors obtained from least-squares fits and do not include systematic errors (see the text for details). Uncertainties for line positions, pressure shift coefficients and their temperature dependences are given in parentheses in units of the last digit quoted. For all other parameters the uncertainty is given in percent in the column immediately to the right of that parameter value.

[a] Positions and their uncertainties are in cm^{-1}.

[b] Line intensities (S) are in cm/molecule at 296 K and scaled by 10^{-24}.

[c] Lorentz half-width coefficients (b_L^0) and pressure shift coefficients (δ^0) are in units of cm^{-1} atm^{-1} at 296 K.
The numbers in each transition entry correspond to air-broadening in the upper row and self-broadening in the lower row.

[d] n_1 and n_2 are the corresponding temperature dependence exponents of air- and self-width coefficients and have no units.

[e] Temperature dependences of pressure shift coefficients, δ'(air) and δ'(self), are in units of cm^{-1} atm^{-1} K^{-1}.

[f] Speed dependence parameter has no units and is assumed to be independent of gas sample temperature and same for both self- and air-broadening.

Table 6

Ro-vibrational, vibrational band intensity, Herman-Wallis parameters and correlation coefficients of measured $^{12}C^{16}O_2$ bands: 6120-6280 cm^{-1}.

Band	Upper State Rotational Constants in cm^{-1}				Intensity Constants			
	G'- G''	B'	$D' \times 10^7$	$H' \times 10^{12}$	$S_V \times 10^{24}$	$a_1 \times 10^4$	$a_2 \times 10^5$	$a_3 \times 10^9$
30013←00001	6227.9166155 (19) 6227.916540(1)[a]	0.3867110194(78) 0.386711076(98)[a]	1.715717 (88) 1.715489(20)[a]	10.234 (26) 0.99(13)[a]	440.610(13)	+3.104 (8)	+1.8624(22)	−0.871(81)
31113←01101 *e* **31113←01101 *f***	6196.176079 (23)	0.386922173 (120) 0.388334478 (121)	1.217528 (135) 1.486159 (155)	−1.930 (19) −1.205 (50)	32.654(5)	+3.26 (5)	+1.087 (26)	0.0 Fixed
32213←02201 *e* **32213←02201 *f***	6170.10837 (43)	0.38860954 (182) 0.38861009 (184)	1.608 (15) 1.458 (15)	0.0 fixed 0.0 fixed	1.254 (4)	0.0 Fixed	0.0 Fixed	0.0 Fixed
40014←10002	6175.11377 (17)	0.38734765 (57)	1.9797 (37)	0.0 fixed	2.247 (4)	−7.97(43)	0.0 Fixed	0.0 Fixed
40013←10001	6205.51034 (28)	0.38555187(165)	0.792 (24)	−12.80 (88)	1.485 (4)	0.0 Fixed	0.0 Fixed	0.0 Fixed
	Lower State Constants							
00001 (fixed)	0.	0.39021894900	1.334088000	0.01918				
01101*e* (fixed) **01101*f* (fixed)**	667.3798265	0.39063910900 0.391254698	1.3539300 1.3616060	2.967 3.040				
02201*e* (fixed) **02201*f* (fixed)**	1335.1313992	0.3916667620 0.3916667620	1.373660 1.381250	−3.765 0.7380				
10001 (fixed) **10002 (fixed)**	1388.1840918 1285.4081123	0.3901889160 0.3904708290	1.149427 1.57157070	1.86596 2.33398				

Band	Correlation Coefficients for Upper State Constants						Correlation Coefficients for Intensity Constants					
	G'- G'' & B'	G'- G'' & D'	G'- G'' & H'	B' & D'	B' & H'	D' & H'	S_V & a_1	S_V & a_2	S_V & a_3	a_1 & a_2	a_1 & a_3	a_2 & a_3
30013←00001	−0.704	−0.540	−0.432	+ 0.938	+ 0.826	+0.958	−0.037	−0.635	+0.058	+0.051	−0.809	−0.072
31113←01101 *e* **31113←01101 *f***	−0.765 −0.764	−0.583 −0.582	−0.460 −0.459	+ 0.931 + 0.930	+ 0.817 + 0.816	+0.958 +0.959	−0.017	−0.756		+0.069		
32213←02201 *e* **32213←02201 *f***	−0.784 −0.779	−0.604 −0.600		+ 0.928 + 0.927								
40014←10002	−0.829	−0.654		+ 0.928			−0.021					
40013←10001	−0.862	−0.758	−0.658	+ 0.966	+0.892	+0.975						

Band	Correlation Coefficients for additional Upper State Constants not listed above									
	B′(e) & B″(f)	***B′(e) & D″(f)***	***B′(e) & H″(f)***	***D′(e) & H″(e)***	***D′(e) & B″(f)***	***D′(e) & D″(f)***	***D′(e) & H″(f)***	***B′(f) & H″(e)***	***D′(f) & H″(e)***	***H′(e) & H″(f)***
31113←01101	+0.585	+0.443	+0.346	+0.958	+0.443	+0.331	+0.255	+0.348	+0.256	+0.195
32213←02201	+0.611	+0.471			+0.471	+0.363				

Notes: The uncertainties reported in parentheses under the various columns correspond to one-sigma internal statistical errors in units of the last quoted digit of the measured values. For example, 6227.916615**5** (19) cm^{-1} corresponds to 6227.916615**5** ± 0.0000019 cm^{-1}.

Contribution due to vibrational partition function for the lower vibrational levels was applied in computing the band strengths listed in the Table above.

The rotational partition function for $^{12}C^{16}O_2$ = 263.87063 [43**]**. A value of 263.60 has been used in this Table to enable comparison with values reported in [**18**] (see **Table 7**).

The band centers and rotational constants are in cm^{-1}. The rotational constants for the lower states (ground state, 01101, 02201, 10001, 10002) are from Refs. **[29-30]**. Note that L**″** (10001) = 0.5663 $\times 10^{-18}$ and L**″** (10002) = −0.9928 $\times 10^{-18}$.

The intensity constants are the same for the *e* and *f* levels of the 31112←01101 and the 32212←02201 bands.

The band strengths (S_V) are in $cm^{-1}/(molecule \cdot cm^{-2})$ x10^{-24} at 296 K.

[a] These ro-vibrational constants are from Ref. [**27**].

The value of S_v (4.4061×10^{-22} cm/molecule at 296 K) reported under intensity constants correspond to the vibrational band strength (S_v) and differs from the sum of all line intensities S_{band} =4.4959×10^{-22} cm/molecule at 296 K (see the text for details).

Table 7

Comparison of measured band intensity[a] parameters for the 30013←00001 and 31113←01101 bands of $^{12}C^{16}O_2$.

Para-meter	30013←00001 band		31113←01101 band	
	Present Study[b]	Toth et al. [**13**]	Present Study[b]	Toth et al. [**13**]
S_v	4.40610 (13) ×10^{-22} 4.4133 (5) ×10^{-22}	4.420 (4) ×10^{-22}	0.32654(5) ×10^{-22} 0.32545 (19) ×10^{-22}	0.3281 (3) ×10^{-22}
a_1	0.3104 (8) ×10^{-3} 0.2880 (11) ×10^{-3}	0.2782 (80) ×10^{-3}	0.326 (5) ×10^{-3} 0.372 (6) ×10^{-3}	0.2308 (248) ×10^{-3}
a_2	0.18624(22) ×10^{-4} 0.1711 (4) ×10^{-4}	0.1826 (26) ×10^{-4}	0.1087 (26) ×10^{-4} 0.1213 (31) ×10^{-4}	0.0482 (98) ×10^{-4}
a_3	−0.871 (81) ×10^{-9}			
N	74	60	136	74
J_{max}	74	67	60	53

[a] Intensities are expressed in units of cm^{-1}/(molecule·cm^{-2}) at 296 K. The uncertainties reported in parentheses under columns 2-5 correspond to one-sigma internal statistical errors in units of the last quoted digit(s) of the measured values. For example, 4.4133 (5) ×10^{-22} corresponds to (4.4133 ± 0.0005) ×10^{-22}.

[b]The upper values in each row under columns 2 and 4 (labeled Present Study) correspond to those from the present study, and the lower values correspond to those determined in Ref. [**18**]. Note that the Herman-Wallis a_3 parameter was not determined in Ref. [**18**] or in Ref. [**13**].

It may be recalled that in the present study the rotational partition function (Q_r) used was 0.12% higher than the value used in [**18**].

Table 8

Off-diagonal relaxation matrix element coefficients, W_{ij}, and their temperature dependence exponents for CO_2-CO_2 and CO_2-air mixing in the 30013 ← 00001 band of $^{12}C^{16}O_2$.

(W_{ij}) between	(W_{ij})[a] CO_2-CO_2	n_2 (W_{ij})[b] (CO_2-CO_2)	(W_{ij})[a] CO_2-air	n_1 (W_{ij})[b] (CO_2-air)
P2 & P4	0.00762(11)		0.00807(13)	
P4 & P6	0.01252(11)		0.01340(14)	
P6 & P8	0.01481(12)	1.002(41)	0.01642(25)	0.883(47)
P8 & P10	0.01784(13)	0.897(42)	0.01951(29)	0.807(48)
P10 & P12	0.02054(14)	0.834(45)	0.02127(31)	0.823(47)
P12 & P14	0.02284(15)	0.889(39)	0.02265(32)	0.815(47)
P14 & P16	0.02510(15)	0.814(37)	0.02230(32)	1.005(47)
P16 & P18	0.02672(16)	0.734(35)	0.02241(33)	1.030(46)
P18 & P20	0.02716(17)	0.900(31)	0.02311(34)	0.924(45)
P20 & P22	0.02739(18)	0.849(26)	0.02313(32)	0.895(38)
P22 & P24	0.02752(19)		0.02347(26)	
P24 & P26	0.02750(21)		0.02226(30)	
P26 & P28	0.02709(24)		0.02042(34)	
P28 & P30	0.02625(27)		0.01664(39)	
P30 & P32	0.02409(30)		0.01452(44)	
P32 & P34	0.02225(35)		0.01128(51)	
P34 & P36	0.02059(41)		0.01071(57)	
P36 & P38	0.01852(48)		0.00497(63)	
P38 & P40	0.01920(56)			
P40 & P42	0.01952(65)			
P42 & P44	0.01986(75)			
P44 & P46	0.02073(86)			
P46 & P48	0.02002(92)			
P48 & P50	0.01447((3)			

R0 & R2	0.00540(7)		0.00249(9)	
R2 & R4	0.01672(11)		0.01041(13)	
R4 & R6	0.02226(11)		0.01634(13)	
R6 & R8	0.02640(11)	0.833(19)	0.01988(21)	0.733(31)
R8 & R10	0.02970(12)	0.814(20)	0.02114(22)	0.913(32)
R10 & R12	0.03159(12)	0.784(20)	0.02227(23)	0.913(33)
R12 & R14	0.03222(12)	0.794(20)	0.02268(23)	0.914(33)
R14 & R16	0.03273(12)	0.822(20)	0.02254(23)	0.973(32)
R16 & R18	0.03239(12)	0.769(20)	0.02300(23)	0.914(31)
R18 & R20	0.03193(13)	0.731(18)	0.02342(23)	0.830(29)
R20 & R22	0.03078(13)	0.676(16)	0.02271(21)	0.855(25)
R22 & R24	0.02894(13)		0.02308(17)	
R24 & R26	0.02800(14)		0.02313(18)	
R26 & R28	0.02681(15)		0.02225(20)	
R28 & R30	0.02592(16)		0.02107(22)	
R30 & R32	0.02512(17)		0.01981(25)	
R32 & R34	0.02229(18)		0.01746(28)	
R34 & R36	0.02104(20)		0.01708(31)	
R36 & R38	0.01978(21)		0.01555(34)	
R38 & R40	0.01796(23)		0.01213(35)	
R40 & R42	0.01579(24)		0.00824(33)	
R42 & R44	0.01155(26)			
R44 & R46	0.00911(26)			
R46 & R48	0.00642(24)			

Notes: The values given in parentheses represent one sigma internal measurement error in units of the last quoted digit.

[a] units are cm^{-1} atm^{-1} at 296 K.

[b] Temperature dependence exponents, n_1 and n_2, have no units (see the text for details).